Sp140L Is a Novel Herpesvirus Restriction Factor

Jana M. Cable[1], Wiyada Wongwiwat[2], Jenna C. Grabowski[1], Robert E. White[2*], Micah A. Luftig[1*]

[1]Duke University School of Medicine, Department of Molecular Genetics and Microbiology, Duke Center for Virology, Durham, NC, USA

[2] Section of Virology, Department of Infectious Disease, Imperial College London, London, United Kingdom

*Co-corresponding authors

Emails: micah.luftig@duke.edu; robert.e.white@imperial.ac.uk

Summary

Herpesviruses, including the oncogenic Epstein-Barr Virus (EBV), must bypass host DNA sensing mechanisms to establish infection. The first viral latency protein expressed, EBNA-LP, is essential for transformation of naïve B cells, yet its role in evading host defenses remains unclear. Using single-cell RNA sequencing of EBNA-LP-Knockout (LPKO)-infected B cells, we reveal an antiviral response landscape implicating the 'speckled proteins' as key restriction factors countered by EBNA-LP. Specifically, loss of *SP100* or the primate-specific *SP140L* reverses the restriction of LPKO, suppresses a subset of canonically interferon-stimulated genes, and restores viral gene transcription and cellular proliferation. Notably, we also identify Sp140L as a restriction target of the herpesvirus saimiri ORF3 protein, implying a role in immunity to other DNA viruses. This study reveals Sp140L as a restriction factor that we propose links sensing and transcriptional suppression of viral DNA to an IFN-independent innate immune response, likely relevant to all nuclear DNA viruses.

Keywords

Herpesvirus, Epstein-Barr virus, EBNA-LP, Herpesvirus Saimiri, Speckled Protein, Sp100, Sp140L, PML Nuclear Bodies, DNA sensors, DNA virus restriction

32 **Introduction**

33 Herpesviruses are double stranded DNA viruses that cause lifelong infections due
34 to their ability to establish viral latency and avoid immunodetection[1]. Clinically relevant
35 herpesviruses include herpes simplex virus (HSV), human cytomegalovirus (HCMV) and
36 Kaposi's sarcoma associated herpesvirus (KSHV), as well as Epstein-Barr virus (EBV),
37 which is associated with numerous lymphomas and carcinomas, and is implicated in
38 several autoimmune disorders – particularly multiple sclerosis[2-4]. The B cell biology of
39 EBV infection and associated diseases can be modeled *in vitro,* as infection of primary B
40 cells leads to cellular transformation and the generation of immortalized lymphoblastoid
41 cell lines (LCLs). Given the ability of herpesviruses to establish lifelong latency, initial
42 infection is a crucial stage where cellular sensing and restriction can prevent the virus
43 from successfully establishing latency. Yet, the mechanisms of intrinsic restriction of
44 herpesviruses have not been fully elucidated.

45 One key mediator of defense against DNA viruses are PML nuclear bodies (PML-
46 NBs), membrane-less nuclear compartments involved in the intrinsic DNA sensing and
47 epigenetic repression of viral chromatin through loading repressive histones and
48 epigenetic modifications on the incoming naked viral DNA genomes[5,6]. Components of
49 PML-NBs can also play a role in the innate antiviral response through inducing expression
50 of interferon-stimulated genes (ISGs)[7-12]. Core PML-NB proteins implicated in restricting
51 DNA viruses include PML, DAXX, ATRX, and Sp100. PML serves as a scaffold to mediate
52 the interaction of other core proteins, while DAXX and ATRX together load the repressive
53 histone variant H3.3 onto viral genomes during initial infection - preventing the
54 accumulation of active histone marks on the incoming viral genome and suppressing the
55 transcription of viral genes[13-17]. HIRA, a separate histone chaperone complex recruited to
56 PML-NBs upon herpesvirus infection[17] and IFN treatment[8,17], also contributes to H3.3
57 deposition on viral chromatin in HSV infection[17,18]. In contrast, H3.3 loading by HIRA at
58 ISG gene loci activates gene expression[7,8]. The speckled protein Sp100, can restrict the
59 replication and viral gene expression of the DNA viruses HSV[19,20], HCMV[21], Human
60 Papilloma Virus[22], and adenovirus[23] when these viruses lack effective countermeasures
61 or when their countermeasures are species-mismatched. Sp100 can bind the
62 heterochromatin protein HP1α[24] and can localize to the promoters of ISGs upon IFN

63 stimulation[10]. However, the mechanisms by which Sp100 restricts DNA virus infection is
64 still unclear.

65 Beyond *SP100*, the speckled protein genetic locus includes additional family
66 members *SP110*, *SP140*, and – exclusively in primates – *SP140L*[25], whose roles in viral
67 infection are largely unknown. The speckled family genes all encode four key domains: i)
68 an N-terminal caspase recruitment (CARD) domain (previously called heterogeneously
69 staining region – HSR) involved in multimerization, ii) the DNA-binding (SAND) "Sp100,
70 AIRE, NucP41/P75 and DEAF" domain, iii) a methyl-histone-binding plant homeodomain
71 (PHD) domain, and iv) a C-terminal acetyl-lysine-binding bromodomain (BRD)[25]. Genetic
72 mutations in *SP110* and *SP140* are associated with autoimmune disorders and increased
73 susceptibility to intracellular bacterial infections[25]. And while Sp110 and Sp140 repress
74 the Type I IFN response in mice[26,27], they appear to promote Type I IFN responses in
75 humans[28]. The *SP140L* gene arose as a likely meiotic crossover event between the
76 *SP100* and *SP140* genes, resulting in a gene combining the 5' CARD domain-encoding
77 region of *SP100* and the remaining protein-encoding domains of the *SP140* gene[29]. The
78 function of Sp140L, however, remains unexplored.

79 To overcome PML-NB restriction, successful herpesviruses encode proteins that
80 antagonize various PML-NB components of their hosts. These include viral tegument
81 proteins belonging to the viral FGARAT homolog family, such as pp71 in HCMV[30,31] and
82 BNRF1 in EBV[32] which target DAXX and ATRX; ORF75 in KSHV which antagonizes
83 DAXX, ATRX, PML, and Sp100[33], and ORF3 of Herpesvirus Saimiri (HVS) – a KSHV-like
84 rhadinovirus of squirrel monkeys – which degrades Sp100[34]. Some immediate-early viral
85 proteins also antagonize PML-NBs, including ICP0 in HSV - a viral E3 ubiquitin ligase
86 which targets PML, Sp100, DAXX, and ATRX[35,36]; IE1 in HCMV targeting PML and
87 Sp100[21,37]; and EBNA-LP in EBV, which transiently displaces Sp100 from PML-NBs
88 during early infection[38,39]. While the molecular mechanism by which these viral proteins
89 antagonize PML-NB components may be distinct, the functional consequences are
90 similar as evidenced by the ability of ICP0 or various combinations of BNRF1 or pp71
91 with IE1 or EBNA-LP to complement an ICP0-null HSV and pp71-deficient HCMV[40-42].
92 The role of Sp100 in EBV infection has not been directly investigated, with studies largely
93 limited to using transient transfection rather than primary infection systems[38,39], and

94 focusing on the shortest Sp100 isoform – Sp100A – which does not contain the SAND,
95 PHD, or Bromo domains, and promotes viral gene transcription, whereas the longer
96 Sp100 isoforms restrict DNA viruses[23,43].

97 EBNA-LP is critical for the transformation of naïve B cells by EBV infection[44], but
98 its function in early infection is not well defined compared to other PML-NB-disrupting
99 herpesvirus proteins mentioned above. The architecture of EBNA-LP is unique in that it
100 is composed of N-terminal, identical, 66 amino acid repeats (W domains) and a C-terminal
101 45 amino acid Y domain. While the structure of EBNA-LP is unknown, it is predicted to be
102 highly disordered[45]. Based on transient transfection assays, EBNA-LP was thought to
103 primarily function as a co-activator of another early EBV protein, EBNA2 to enhance
104 expression of the essential viral gene Latent Membrane Protein 1 (LMP1) and some
105 cellular genes[46-50]. The mechanism by which EBNA-LP co-activates EBNA2 has been
106 variously attributed to displacement of the transcriptionally repressive HDAC4 and NCoR
107 proteins from viral and cellular promoters[51,52]. However, B cells infected with an EBNA-
108 LP Knockout EBV (LPKO) exhibit reduced expression of not only LMP1, but also other
109 viral genes that are not EBNA2-dependent, while EBNA2-induced host gene expression
110 is not reduced, or even increased, in the absence of EBNA-LP during infection[44]
111 suggesting that EBNA-LP's relationship to EBNA2 is more complex than a simple
112 'coactivator'. Additionally, our recent work identified highly conserved, hydrophobic
113 leucine-rich motifs in both the W and Y domains of EBNA-LP that associate with the DNA-
114 looping factor YY1[53]. Thus, EBNA-LP likely has EBNA2-independent roles that are critical
115 for establishing latency in, and transformation of, naïve B cells.

116 Given the essential role of immediate-early herpesvirus proteins in overcoming
117 intrinsic viral restriction, and particularly the gap in knowledge as to how and why EBNA-
118 LP is necessary for EBV infection and transformation of naïve B cells, we used single cell
119 RNA-sequencing (scRNAseq) to compare the trajectories of wild type (WT) and LPKO
120 virus infected B cells during the first days of infection. This assay revealed key facets of
121 the restriction of EBV in the absence of EBNA-LP. We then defined the cellular factors
122 and mechanisms responsible for the restriction of the LPKO virus, and finally the breadth
123 of how these factors are restrictive across human DNA viruses.
124

125 # Results

126 ## EBNA-LP Dictates the Fate Trajectories of EBV-Infected B Cells

127 To assess the role of EBNA-LP in EBV-driven B cell fate trajectories, we performed
128 single cell RNA sequencing (scRNAseq) of primary human B cells prior to infection (Day
129 0), and at 2, 5, and 8 days following WT and LPKO infection as depicted in **Figure 1A**. B
130 cell purity (**Figure S1A**) and infection efficiency (**Figure S1B**) were confirmed by
131 expression of CD19 and CD23 respectively at time of collection. Single cell RNA-seq
132 revealed that infected samples contained more mRNA (**Figure S1C**) and more unique
133 mRNA features (**Figure S1D**) per cell than uninfected (Day 0) B cells. Dimensional
134 reduction integrating all seven samples generated a single UMAP for further analysis
135 (**Figure 1B**). Uninfected cells largely cluster separately from infected cells (**Figure 1C**)
136 and 2 days post-infection LPKO- and WT-infected clusters are nearly identical to each
137 other (**Figures 1D and 1E**). Differences in cellular states between WT- and LPKO-
138 infected B cells emerge by 5 days (**Figures 1F and 1G**) and are accentuated 8 days post-
139 infection (**Figures 1H and 1I**).

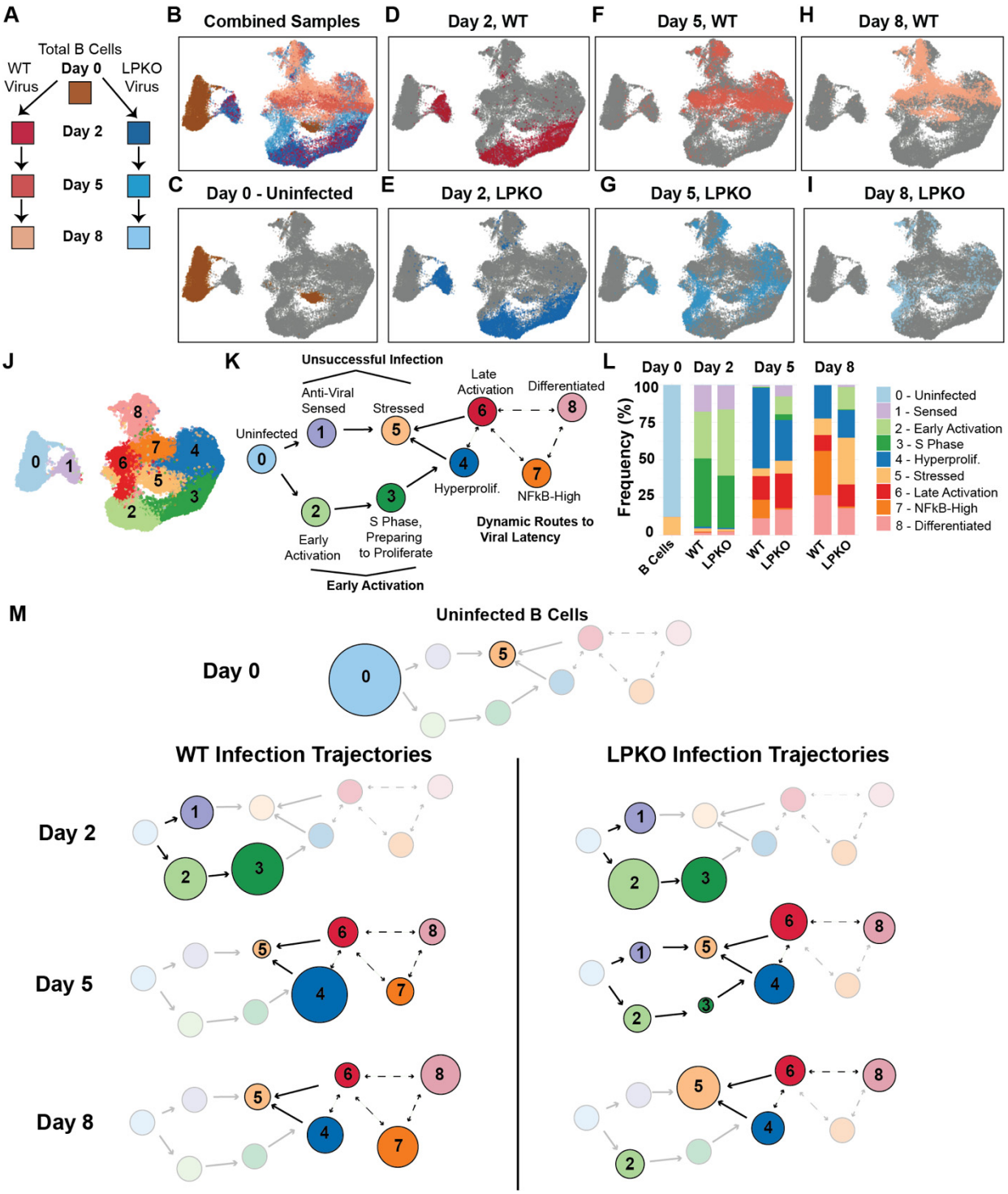

Figure 1. LPKO-infected B cells have altered cellular trajectories compared to WT EBV. (**A**) Schematic of collected samples. (**B**) Uniform Manifold Approximation and Project for Dimension Reduction (UMAP) of the combined seven samples. Colors correspond to samples in (**A**). (**C**) UMAP with uninfected B cells highlighted. (**D**) Cells 2 days post-infection with WT. (**E**) Cells 2 days post-infection with LPKO. (**F**) Cells 5 days post-infection with WT. (**G**) Cells 5 days post-infection LPKO. (**H**) Cells 8 days post-infection WT. (**I**) Cells 8 days post-infection LPKO. (**J**) UMAP with cells grouped into 9 unique clusters based on differential gene expression. (**K**) Model of the identified clusters in the cellular trajectories of EBV infected B cells. (**L**) Frequency of each cluster within each sample. (**M**) Model of the trajectories of WT- and LPKO-infected B

cells at each time point based on frequencies in (**L**). Circle area is proportional to frequency of cluster in each sample. Transparent circles represent clusters which are absent.

Our prior work defined a set of distinct B cell fate trajectories following EBV infection that largely mimic the states of B cell activation and germinal center maturation[54]. In comparing WT- and LPKO-infected cells, we have identified 9 distinct cell states that largely recapitulated those characterized previously (**Figure 1J and Table S1**). We used the top cluster-defining genes in our previous study to identify the corresponding cell states in this dataset (**Figures S2A-S2I**). Cell states were further distinguished on the basis of viral gene expression (**Figures S2J-S2U**) and cell cycle phase (**Figures S2V-S2X**). Cluster 0 (Uninfected – c0) contained uninfected naïve and memory B cells (**Figure 1K**). Two days post-infection, prior to cellular proliferation, which begins around 3 days post-infection[55], a portion of cells exist in a gene expression state associated with antiviral sensing (Sensed – c1) (**Figure 1K**). Cells that avoid this initial barrier transition towards an activated state, resembling pre-germinal center B cells (Early Activation – c2), and towards a state of DNA replication enriched for cells in S phase (S Phase – c3) (**Figure 1K**). By 5 days post-infection, cells advanced to a state of hyperproliferation, with markers of dark zone germinal center B cells (Hyperproliferating – c4) (**Figure 1K**). Likely as a result of the cellular stress associated with EBV-induced hyperproliferation[55,56], by this time point some cells also arrest in a state of cellular stress (Stressed – c5) (**Figure 1K**). Cells also transition towards a second, but distinct, activated B cell state (Late Activation – c6) (**Figure 1K**). Compared to the Early Activation state (c2), this Late Activation state (c6) is more highly enriched in naïve B cells based on IgD expression (**Figure S2X**), has lower expression of Myc and E2F targets (**Figures S2Y and S2Z**) likely a consequence of reduced expression of the viral transactivator EBNA2 in c6 compared to c2[57] (**Figure S2R**), and is likely dependent upon cells having undergone proliferation based on its appearance only after day 2 (**Figure 1K**). EBV-infected cells also enter a NFκB-High state, likely driven by the viral protein LMP1, whose expression is highest in this population (**Figure S2T**), that is characterised by markers of light zone germinal center B cells (NFκB High - c7) (**Figure 1K**). The final population is a differentiated plasmablast-like state (Differentiated - c8) (**Figure 1K**).

180 While this model held true for WT-infected cells, LPKO-infected cells had altered
181 trajectories. First, unlike WT-infected cells, LPKO-infected cells remain in the early (pre-
182 proliferation) states of activation (c2 and c3) beyond 2 days post infection (**Figure 1L**).
183 Second, LPKO-infected cells were also more likely than WT-infected cells to enter states
184 of antiviral sensing (c1) or cellular stress (c5) after day 2 (**Figure 1L**). Finally, the LPKO-
185 infected cells largely failed to establish the NFκB-High state (c7) (**Figure 1L**), consistent
186 with the previously reported low expression of LMP1 in LPKO infections[44] (**Figure S2U**).
187 Surprisingly, the LPKO virus efficiently established the plasmablast state (Differentiated –
188 c8) (**Figure 1L**), despite the absence of the NFκB-High state which is critical in the
189 emergence of plasmablasts from the germinal center[58]. Interpreted as trajectories in
190 **Figure 1M**, LPKO-infected cells persist in early infection states of activation (c2 and c3)
191 and cellular stress prior to proliferation (c1) longer than WT. LPKO-infected cells that do
192 hyperproliferate, have a higher propensity to arrest with signs of cellular stress (c5) and
193 to enter a germinal center- or light zone-independent route towards the plasmablast state
194 (c8), similar to germinal center-independent B cell maturation[59].
195 To validate our transcriptome data, we first identified RNA changes in cell surface
196 markers defining the key cell populations. RNA levels of CCR6 (**Figure 2A**) and CD23
197 (**Figure 2B**) in the scRNA-seq data distinguish many cell states, similar to previous
198 studies[54]. Early Activation states (c2 and c3) are characterized by $CCR6^{hi/}CD23^{lo}$
199 expression, while the Late Activation state (c6) is $CCR6^{hi/}CD23^{hi}$. The NFκB-High state
200 (c7) is $CCR6^{lo}/CD23^{hi}$ and is further resolved by high expression of ICAM1 (**Figure 2C**),
201 a proxy marker for LMP1 expression [60]. The remaining states are $CCR6^{lo}/CD23^{lo}$ with the
202 Stressed (c5) distinguishable from the Differentiated state (c8) by low expression of CD38
203 (**Figure 2D**) and reduced cellular proliferation. Therefore, these markers along with the
204 proliferation tracker CellTrace should allow quantitation of the main states that differ
205 between LPKO and WT infections: persistence in states of activation (c2, c3, c6), reduced
206 transition to the NFκB-high state (c7), and increased cellular arrest prior to
207 hyperproliferation (c5) as outlined in **Figure 2E**.

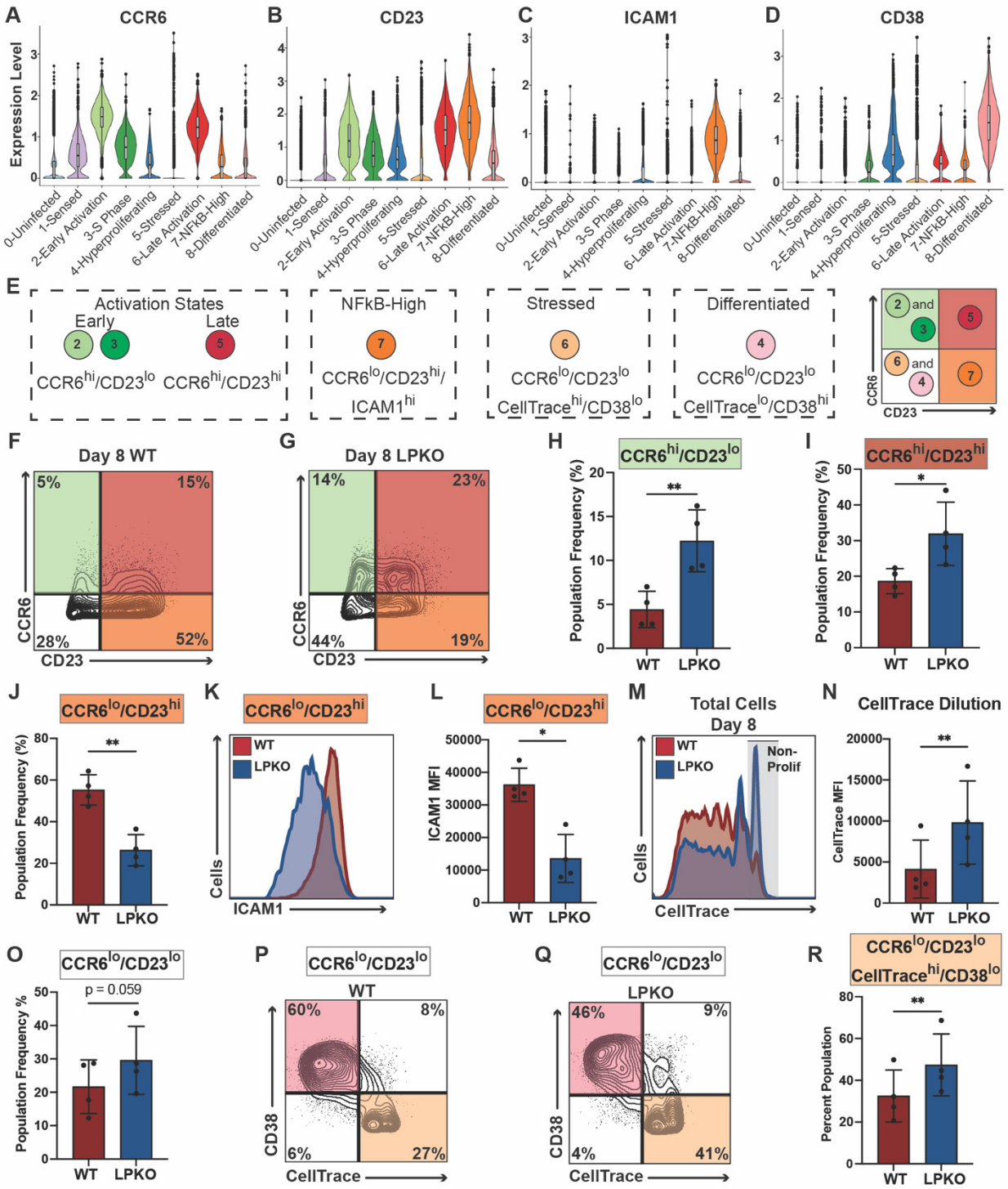

Figure 2. Altered cell populations between WT- and LPKO-infected B cells identified in scRNAseq data are validated by flow cytometry 8 days post-infection. Expression levels of CCR6 (**A**), CD23 (**B**), ICAM1 (**C**), and CD38 (**D**) in scRNA-seq clusters. (**E**) Legend of flow panel marks for the key states identified. Flow staining for CCR6 and CD23 8 days post-infection in representative Donor 2 for WT (**F**) and LPKO (**G**) infected B cells. Quadrant color corresponds to cell states that can be distinguished as depicted in (**E**). Percent of WT- and LPKO- infected cells 8 days post-infection in the CCR6^{hi}/CD23^{lo} (Early Activation) states (**H**), the CCR6^{hi}/CD23^{hi} (Late Activation) state (**I**), and the CCR6^{lo}/CD23^{hi} (NFκB-High) states (**J**). (**K**) Histogram comparing expression of ICAM1 protein (proxy for LMP1) between WT and LPKO infected cells

in CCR6^{lo}/CD23^{hi} population. (**L**) Quantified Median Fluorescence Intensity (MFI) of ICAM1 signal in CCR6^{lo}/CD23^{hi} population in WT and LPKO infections (n = 4). (**M**) Histogram of CellTrace stain, diluted during each cell division, 8 days post infection in WT and LPKO infected cells in representative Donor 1. Grey area indicates cells that have not proliferated. (**N**) MFI of CellTrace (n=4). Lower MFI indicates more cell proliferation. (**O**) Percent of WT and LPKO infected cells 8 days post-infection in the CCR6^{lo}/CD23^{lo} states (n=4). Separation of CCR6^{lo}/CD23^{lo} populations in WT (**P**) and LPKO (**Q**) infection by CD38 and CellTrace to distinguish Differentiated cells from Stressed cells. (**R**) Percent of CCR6^{lo}/CD23^{lo} cells that are also CD38^{lo} and CellTrace^{hi} (indicating low proliferation) representing the stressed cell cluster. Significance determined with ratio paired t test. N = 4 biological replicates. *Indicates p value less than or equal to 0.05, ** indicates p value less than or equal to 0.01. Histograms are scaled as percent of maximum count (modal).

Using Flow cytometry to analyze protein expression of identified markers in a new set of infected samples, we classified cells by CCR6 and CD23 levels (**Figures 2F, 2G, S3A, and S3B**) and confirmed the prolonged presence of LPKO-infected cells in states of early activation (c2 and c3) (CCR6^{hi}/CD23^{lo}) (**Figure 2H**) and late activation (c6) (CCR6^{hi}/CD23^{hi}) (**Figure 2I**) compared to WT infection. Second, we confirmed that LPKO-infected cells have reduced transition to NFκB-high state (c7), as LPKO-infected cells have reduced CCR6^{lo}/CD23^{lo} populations (**Figure 2J)** and the cells that do enter this state express significantly less ICAM1 **(Figures 2K, 2L, and S3C)** compared to WT. Furthermore, compared to WT, LPKO-infected cells are less proliferative (**Figures 2M, 2N, and S3D).** And, upon further separating CCR6^{lo}/CD23^{lo} cells based on CD38 expression and proliferation, we confirmed that compared to WT, LPKO-infected cells are more frequently in states of cellular stress (c5) (CCR6^{lo}/CD23^{lo}/CellTrace^{hi}/CD38^{lo}) (**Figures 2O-2R, S3E, and S3F**). Altogether, these data support a model in which EBNA-LP is important in preventing the arrest, stress response, and immune activation after EBV infection.

LPKO-Infected Cells Fail to Suppress the Antiviral Response and Fail to Induce Cellular Metabolic Remodeling

We next sought to characterize the molecular mechanisms underlying the cell fate restrictions following LPKO infection. We first pooled all time points for each WT and LPKO scRNAseq dataset into a “pseudo-bulk” dataset and performed gene set enrichment analysis (GSEA) to identify differentially regulated pathways between WT and LPKO infection. In WT-infected cells, we observed significant enrichment of transcripts involved in NFκB signaling (**Figure 3A**) in agreement with the failure of LPKO-infected

cells to generate an NFκB-high state (**Figure 1L**). We also observed an increase in expression of genes controlling cellular metabolism in WT- relative to LPKO-infected cells (**Figure 3A**). In contrast, LPKO-infected cells were enriched for transcripts of interferon-stimulated genes (ISGs) and antiviral responses (**Figure 3B**).

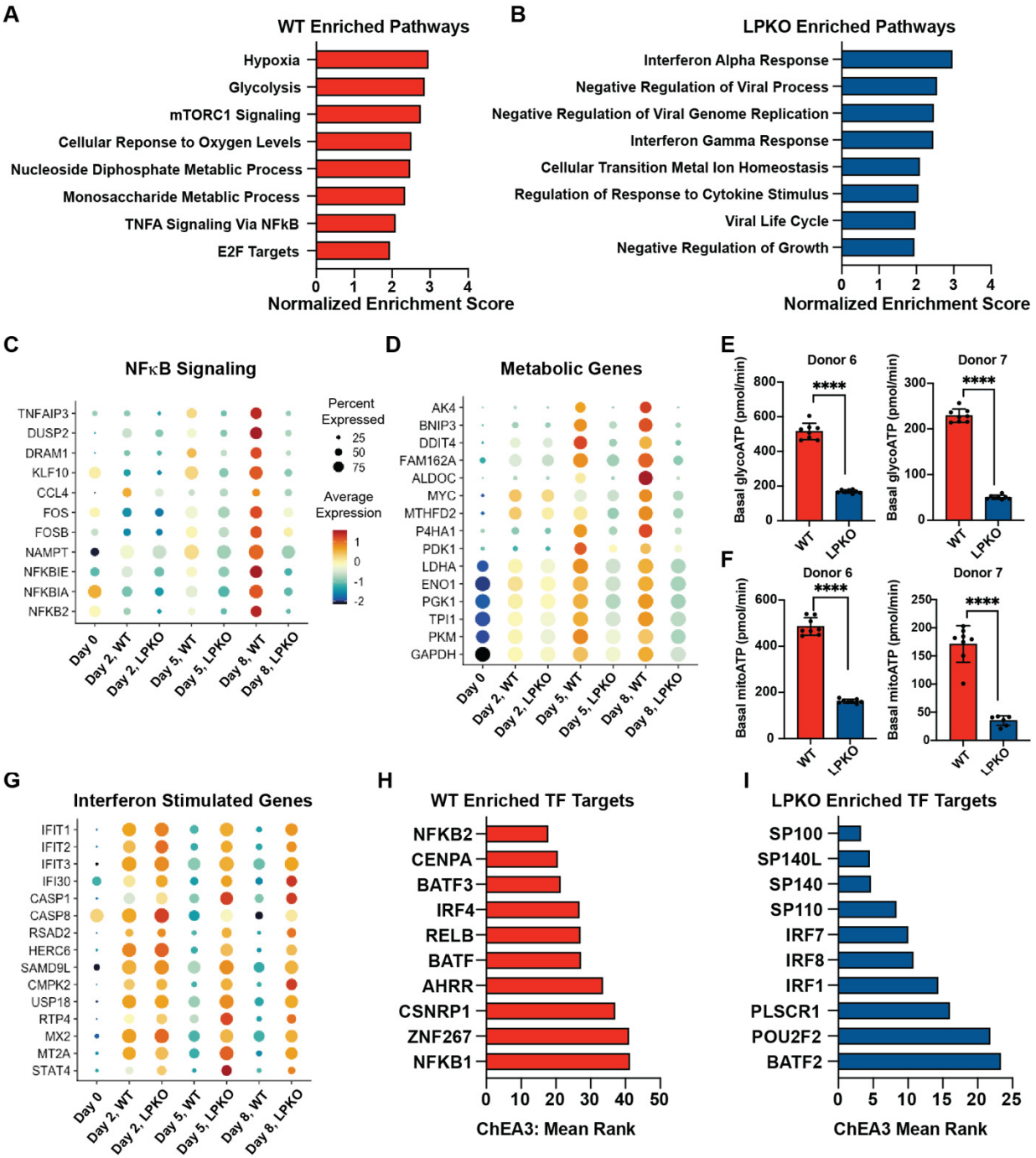

Figure 3. EBNA-LP promotes expression of pro-proliferative genes, while reducing expression of anti-viral genes. Pathways identified as enriched in WT- compared to LPKO- (**A**) or LPKO- compared to WT- (**B**) infected scRNAseq samples by GSEA Hallmark gene sets or Gene Ontology datasets. Representative top-ranking pathways with false discover rates (FDR q-values) less than 0.05. Higher

normalized enrichment score indicates stronger enrichment. Dot plot of representative NFκB signaling-related genes (**C**) and metabolism genes (**D**) identified in GSEA pathways enriched in WT infected cells for each sample in the scRNAseq time course. (**E**) Basal rate of ATP derived from glycolysis (glycoATP) in WT- and LPKO-infected naïve B cells 4 days post-infection in two donors. (**F**) Basal rate of ATP derived from oxidative phosphorylation (mitoATP) in WT- and LPKO-infected naïve B cells 4 days post-infection in two donors. (**G**) Dot plot of representative Interferon Stimulated Genes enriched in LPKO-infected cells for each sample in the time course. (**H**) Top ten predicted transcription factors identified by ChEA3 associated with expression of the genes enriched in WT-infected cells in scRNAseq samples compared to LPKO or (**I**) LPKO-infected cells compared to WT. Lower mean rank indicates a stronger correlation.

We next used time-resolved pseudo-bulk analysis to better define the dynamic nature of EBNA-LP-dependent gene regulation. NFκB targets were modestly decreased 2 days post-infection in both WT and LPKO-infected cells, but then diverged at 5, and more so at 8, days post infection (**Figure 3C**). Cellular metabolic gene expression diverged by day 5, following the first EBV-induced cell division (**Figure 3D**). While loss of NFκB signaling is concurrent with failure to efficiently expression LMP1 [44] (**Figure S2U**), failure to upregulate cellular metabolism in the absence of EBNA-LP was previously unexplored. Therefore, we further examined cellular metabolic activity during early infection and confirmed naïve B cells infected with LPKO virus had reductions in both basal glycolysis and oxidative phosphorylation compared to WT infected cells at 4 days post-infection (**Figures 3E and 3F**).

Transcripts downregulated upon expression of EBNA-LP (i.e. induced in LPKO-infected cells) were primarily ISGs. Intriguingly, though, interferon gene mRNAs were not elevated in LPKO-infected cells (**Figure S4A**), indicating ISG induction may occur through other mechanisms. These ISG transcripts are widely induced by two days post-infection in both WT- and LPKO-infected cells (**Figure 3G**). In the presence of EBNA-LP, WT-infected cells effectively down-regulated expression of these ISGs, whereas in LPKO-infected cells, levels of these ISG transcripts were sustained or increased (**Figure 3G**). These trends in differentially expressed pathways observed in the scRNAseq data were confirmed by bulk RNAseq of WT- and LPKO-infected cells in additional donors at 8 days post-infection (**Figures S4B-S4F**).

Because the ISG induction appeared to be independent of IFN induction, we sought to identify which cellular factors could be mediating the observed gene expression differences in WT- and LPKO-infected cells. We used ChEA3[61] (ChIP-X Enrichment Analysis Version 3) to identify transcription factors whose target genes were enriched in

296 the transcriptome of WT- and LPKO-infected cells. Genes upregulated in WT-infected
297 cells were associated with factors including NFκB subunits; CENPA – a centromere
298 protein and transcriptional regulator that forms a complex with YY1[62] which we recently
299 identified as an EBNA-LP-interacting protein[53]; and IRF4, which can suppress ISG
300 transcription[63], induce expression of Myc[63,64], and function in cooperation with BATF and
301 BATF3 that are also suggested mediators of these expression changes by the
302 analysis[65,66] (**Figure 3H**). Genes upregulated in the absence of EBNA-LP were instead
303 associated with all four human speckled proteins (Sp100, Sp110, Sp140, and Sp140L)
304 (**Figure 3I**).
305
306 **Sp100 and Sp140L, but Not Other PML-NB Proteins, are Required to Restrict EBV**
307 **Transformation in the Absence of EBNA-LP**
308 To examine whether the ChEA3-identified speckled proteins or other PML-NB
309 proteins specifically restrict EBV infection in the absence of EBNA-LP, we assessed the
310 effect of knocking out these target genes on rescuing the inability of LPKO virus to
311 transform naïve B cells. Naïve B cells isolated from adult peripheral blood (**Figure S5A**)
312 were directly transfected with Cas9-guide RNA ribonucleoprotein (Cas9/RNP) complexes
313 targeting genes encoding the main components of PML bodies, including the speckled
314 proteins, along with CD46, a non-essential cell surface protein used as a proxy for
315 knockout of the target gene[67] (**Figure 4A**). Transfected cells were then infected with either
316 the LPKO or WT virus, and outgrowth of edited, CD46-negative cells was assessed by
317 flow cytometry weekly post-infection, for 4 weeks (**Figure 4A**). As expected, control
318 LPKO-infected cells in which only *CD46* was targeted failed to sustain proliferation to
319 generate LCLs, whereas WT EBV still transformed the naïve B cells into LCLs (**Figures**
320 **4B-4D**). While knockout of most of the PML-NB-associated proteins that were targeted –
321 including *PML* – had no significant impact on the outgrowth of LPKO-infected cells, which
322 decreased in number over time like the *CD46*-only knockout, mutation of either *SP100* or
323 – even more emphatically – *SP140L* rescued outgrowth (**Figures 4B and 4C**). Indeed,
324 knockout of *SP100* or *SP140L* was sufficient to consistently generate LPKO LCLs by 28
325 days post-infection (**Figure 4D**) and target genes were efficiently knocked out in these
326 LCLs as validated by genomic DNA sequencing (**Figure S5B**) and protein expression

where applicable (**Figure S5C**). Additional LPKO LCLs were generated after a longer time in culture with inconsistent target knockout (**Figure S5D**), likely arising from contaminating memory B cells. Targeting the same factors in WT infected cells had no impact on outgrowth (**Figures S5E and S5F**), confirming Sp100 and Sp140L restrict EBV infection only in the absence of EBNA-LP.

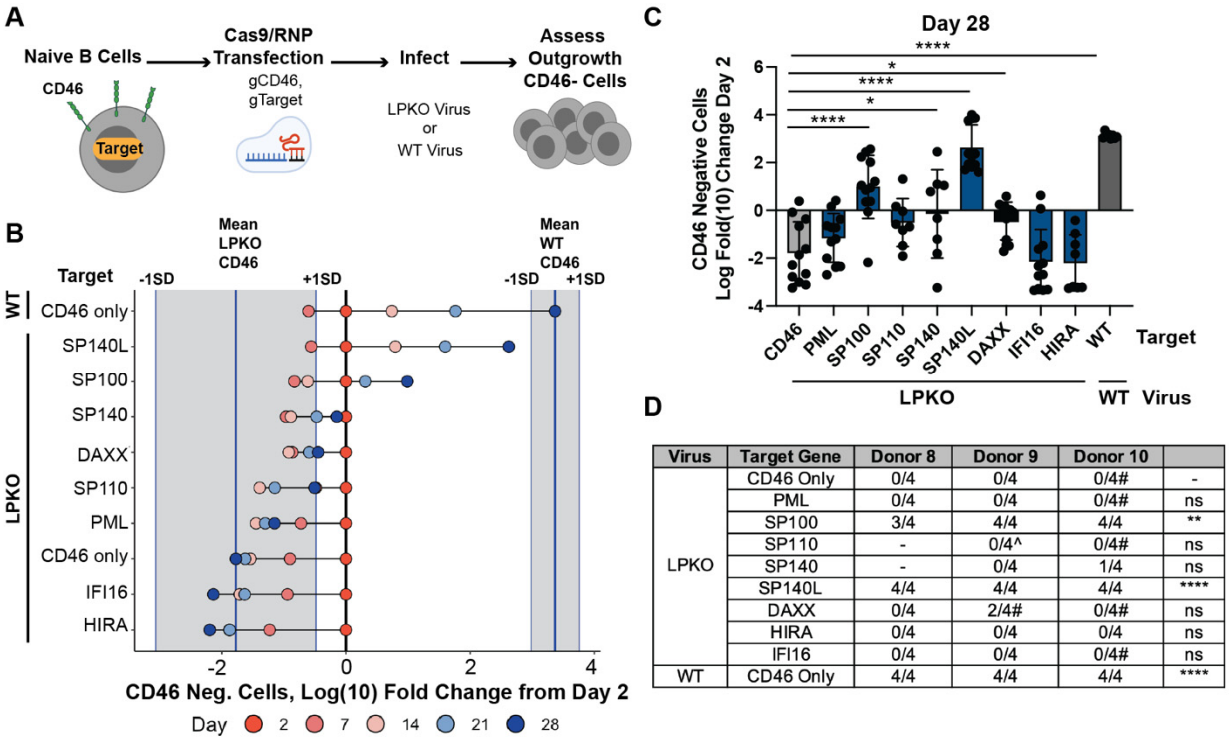

Virus	Target Gene	Donor 8	Donor 9	Donor 10	
LPKO	CD46 Only	0/4	0/4	0/4#	-
	PML	0/4	0/4	0/4#	ns
	SP100	3/4	4/4	4/4	**
	SP110	-	0/4^	0/4#	ns
	SP140	-	0/4	1/4	ns
	SP140L	4/4	4/4	4/4	****
	DAXX	0/4	2/4#	0/4#	ns
	HIRA	0/4	0/4	0/4	ns
	IFI16	0/4	0/4	0/4#	ns
WT	CD46 Only	4/4	4/4	4/4	****

Figure 4. Knockout of *SP140L* or *SP100* rescues transformation of LPKO-infected naïve B cells. (**A**) Schematic of Cas9/RNP screening approach. (**B**) Log(10) Fold Change from Day 2 of the total number of CD46 negative cells for each condition 2, 7-, 14-, 21-, and 28-days post-infection. Dark turquoise line represents the mean number of CD46 negative cells in CD46 only control WT- or LPKO- infected cells 28 days post infection. SD = standard deviation. (**C**) Total number of CD46 negative cells 28 days post infection for each condition plotted as log fold change from 2 days post infection. P values calculated by one-way ANOVA with multiple comparisons to compare to LPKO infected cells transfected with guide targeting CD46 only as control. *Indicates p-values <0.05, ** indicates p-values <0.01, **** indicates p value < 0.0001. (**D**) Total number of LPKO LCLs in each donor for each target out of 4 replicates per donor. #Indicates conditions in which at least one LCL was generated after an additional three weeks in culture with variable knockout efficiency. ^Indicates conditions in which at least one LCL was generated in the same time frame at WT virus, but target gene was not knocked out. P values calculated using Fischer's exact test to compare outcomes to LPKO control condition ** indicates p-values <0.01, **** indicates p value < 0.0001.

Structural characterization of EBNA-LP/Sp140L and Sp100 interactions define a critical interface important for B cell transformation

To better understand the nature of the putative interaction between EBNA-LP and Sp140L and Sp100, we used Alphafold3 to predict the structure of a complex between

352 these proteins[68]. First, we found that despite EBNA-LP being predicted to have high
353 intrinsic disorder[45], AlphaFold3 consistently predicted that EBNA-LP forms an extended
354 beta sheet, with loops connecting helices derived from the repeated W domains and a
355 loop extending the unique 45 amino acid Y domain containing a short alpha helix (**Figures**
356 **5A and 5B**). The interaction sites with Sp140L and Sp100 are consistently predicted to
357 involve this Y domain alpha helix engaging a CARD domain derived helical bundle of
358 Sp140L and Sp100 (**Figure 5C and 5D**), the latter being consistent with prior biochemical
359 findings[38]. Specifically, the hydrophobic interface of these interactions relies on a
360 conserved leucine rich motif (LRM) within EBNA-LP[53] (**Figures 5E and 5F**).
361 To examine the role of the Y domain LRM at the speckled protein interface in
362 transformation of naïve B cells, we used a trans-complementation assay in cord blood B
363 cells infected with LPKO virus as previously described[53]. Prior to infection, cells were
364 transfected with an episomal plasmid encoding tdTomato and either wild type or an
365 EBNA-LP mutant in which leucines were mutated to alanine. EBNA-LP with a mutated Y
366 domain LRM failed to rescue transformation of LPKO-infected cord blood B cells
367 compared to wild-type EBNA-LP (**Figures 5G – 5I**) – suggesting the Y domain LRM motif
368 of EBNA-LP is essential during EBV infection.

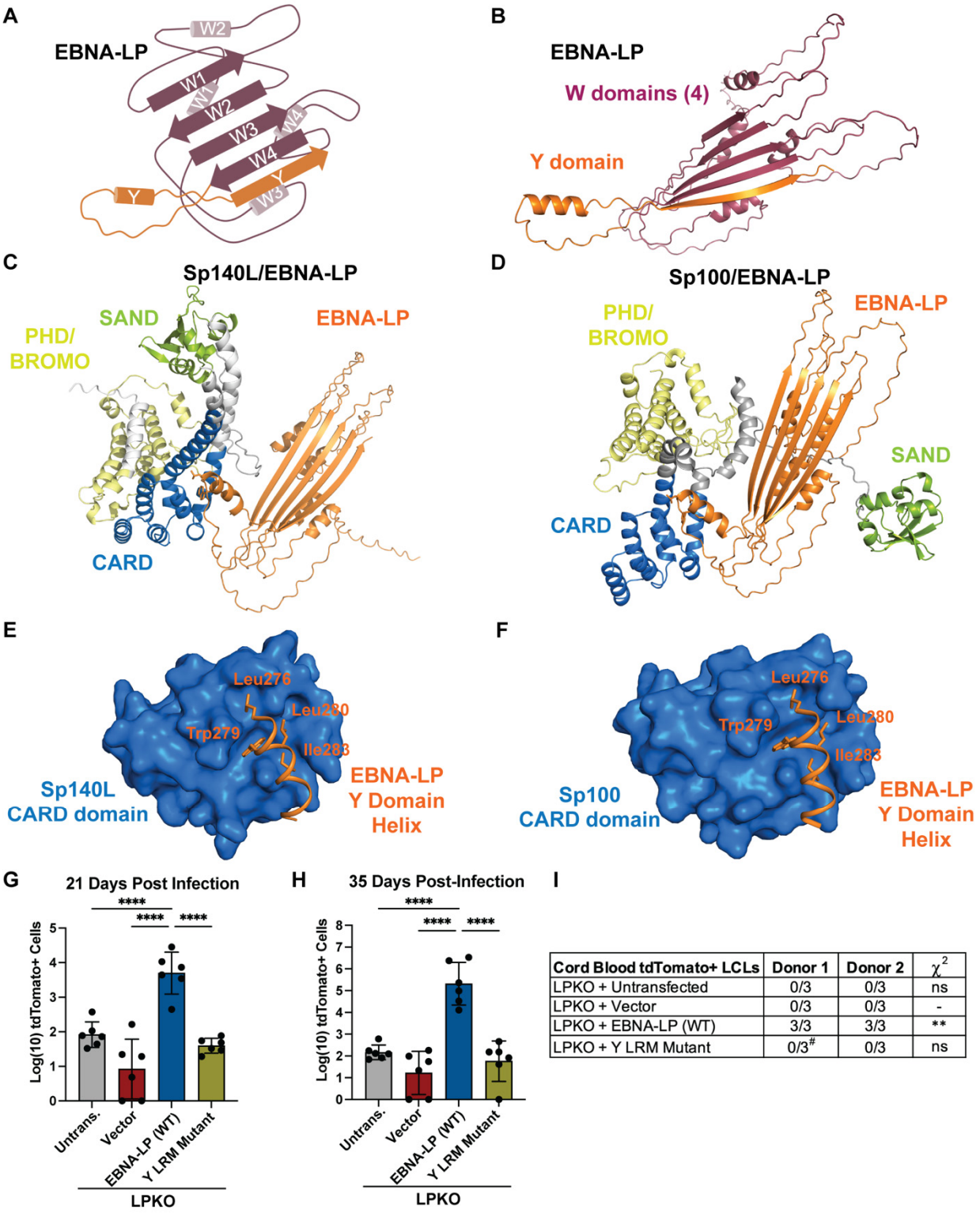

Cord Blood tdTomato+ LCLs	Donor 1	Donor 2	χ^2
LPKO + Untransfected	0/3	0/3	ns
LPKO + Vector	0/3	0/3	-
LPKO + EBNA-LP (WT)	3/3	3/3	**
LPKO + Y LRM Mutant	0/3#	0/3	ns

Figure 5. EBNA-LP is predicted to engage Sp140L and Sp100 through an alpha-helix containing a leucine-rich motif in the C-terminal Y domain. (**A**) Schematic of EBNA-LP (encoding 4 repeated W domains) predicted structure W (magenta) and Y domain (orange) contributions to beta strands and alpha helices based on **B**. (**B**) Alphafold3-predicted model of EBNA-LP three-dimensional structure. Predicted model of EBNA-LP (orange) in complex with (**C**) Sp140L and (**D**) in complex with Sp100. Speckled protein domains are highlighted: CARD domain (blue), SAND domain (green), PHD/BROMO domain (yellow).

Zoomed in view of EBNA-LP Y domain helix (spanning amino acids 276 through 287) encoding the leucine-rich motif in contact with (**E**) Sp140L and (**F**) Sp100 CARD domains. EBNA-LP residues with side-chains predicted to contact CARD domains are indicated. Total tdTomato positive cells in each condition of cord blood B cells infected with LPKO and trans-complemented with indicated DNA construct (**G**) 21 days post-infection and (**H**) 35 days post-infection (performed in two donors, with 3 replicates each). Untransfected cells indicates background signal threshold. P values calculated by ordinary one-way ANOVA with Dunnett's multiple comparisons test. **** Indicates p value < 0.0001. (**I**) Number of tdTomato positive LCLs generated per condition. # Indicates a single replicate in which cells were transformed but were not tdTomato positive. P values were calculated using Fisher's exact test to compare transformation outcomes to LPKO-infected cells trans-complemented with empty vector. ** Indicates p value < 0.01.

***SP100* or *SP140L* Knockout Rescues Cellular and Viral Gene Expression Critical for Naïve B Cell Outgrowth**

We then sought to investigate the mechanism by which Sp100 and Sp140L restrict EBV infection in the absence of EBNA-LP. We used bulk RNAseq to examine the effect of *SP100* and *SP140L* knockout on viral and cellular gene expression five days after LPKO infection of naïve B cells (**Figure S6A**). Knockout of *SP100* or especially *SP140L* reduced induction of IFN-related genes in LPKO-infected cells (**Figures 6A-6D**). Knockout of either *SP100* or *SP140L* also rescued the expression of pathways important for proliferation including MYC targets, E2F targets, and particularly upon *SP140L* knockout, metabolic pathways (**Figures 6A-6C and 6E**). NFκB signaling was also rescued by *SP100* and *SP140L* knockout in LPKO infected cells (**Figures 6A-6C and 6F**), with knockout of *SP140L* again exhibiting in a more complete rescue of gene expression towards wild-type levels – in agreement with the transformation screen (**Figure 4B**). Since LMP1 and other viral genes are inefficiently activated during LPKO infection[44], we examined viral latency gene expression, and found that *LMP1* and *LMP2* RNA levels in LPKO infected cells were somewhat elevated upon loss of *SP100* and largely recovered in *SP140L* knockouts (**Figure 6G**). This was further confirmed at a functional level by flow cytometry using ICAM1 as a proxy for LMP1, as knockout of *SP100* or – to a greater extent – *SP140L* rescued surface ICAM1 protein to levels comparable to WT infected cells (**Figures 6H and S6B**).

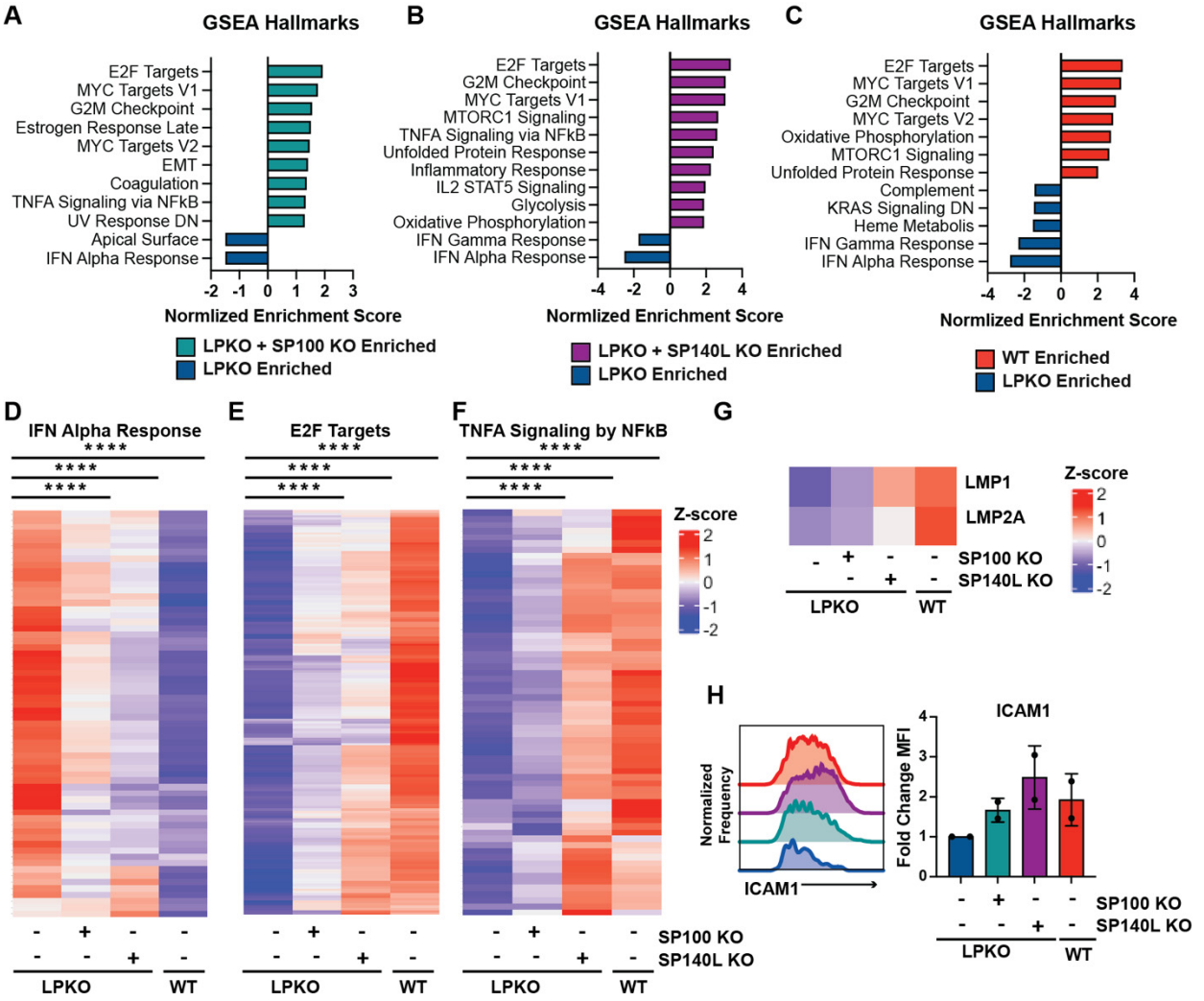

Figure 6. *SP100* and *SP140L* Knockout in LPKO-infected cells promotes transcription of pathways required for outgrowth and inhibits the anti-viral response. GSEA Hallmark pathway analysis of bulk RNA-sequencing samples 5 days post-infection comparing LPKO infected cells with (**A**) *SP100* knockout, (**B**) *SP140L* knockout or WT virus infection (**C**) to in comparison control LPKO infection (n = 2). GSEA terms with nominal p value less than 0.05 are shown. Higher absolute value of the normalized enrichment score indicates stronger enrichment. Heatmap of genes related to the significantly enriched Hallmark pathways (**D**) "Interferon (IFN) Alpha Response," (**E**) "E2F Targets", and (**F**) "TNFA Signaling by NFκB" for each condition. Average z-score of two samples is plotted. P values determined by One-way Repeated Measures ANOVA with multiple comparisons to LPKO control. **** indicates p value less than 0.0001. (**G**). Average Z-score for mRNA encoding LMP1 and LMP2A for each sample. (**H**). Histogram of flow cytometry signal for LMP1 proxy gene ICAM1 in each sample.

Sp140L Also Restricts ORF3-Deficient Herpesvirus Saimiri (HVS)

As Sp140L has not previously been studied as a viral restriction factor, we sought to determine whether Sp140L can restrict herpesviruses other than EBV, and in cell types other than B cells, by studying Sp140L in HVS infection. As the HVS tegument protein

426 ORF3 targets Sp100 for degradation[34], we generated two independent WT HVS and
427 ORF3-KO HVS viruses (**Figure S7A and 7B**) carrying a CMV promoter-driven luciferase
428 expression cassette. We confirmed infection of human fibroblast HFF cells with WT HVS,
429 but not ORF3-KO HVS, resulted loss of Sp100 protein (**Figure S7C**). We then compared
430 virus transcription after initial infection in two human fibroblast cell lines (HFF and MRC5
431 cells) carrying knockout of either *SP100* or *SP140L* alongside the proxy gene *CD46*
432 (**Figure 7A**). Consistent with a previous report with an ORF3-KO of a C-strain HVS[34],
433 knockout of *SP100* rescued viral transcription after ORF3-KO HVS infection (**Figures 7B**
434 **and 7C**). Consistent with our EBV data, knockout of *SP140L* was also sufficient to rescue
435 luciferase expression from the ORF3-KO virus in both cell types (**Figures 7B and 7C**).
436 Loss of *SP100* or *SP140L* in the context of WT HVS infection had little or no effect on
437 viral transcription (**Figures S7D-7F**) suggesting that ORF3 antagonizes both Sp100 and
438 Sp140L function during WT HVS infection. These findings suggest Sp140L is a restriction
439 factor of diverse gammaherpesviruses in primates, that is at least as important as Sp100.

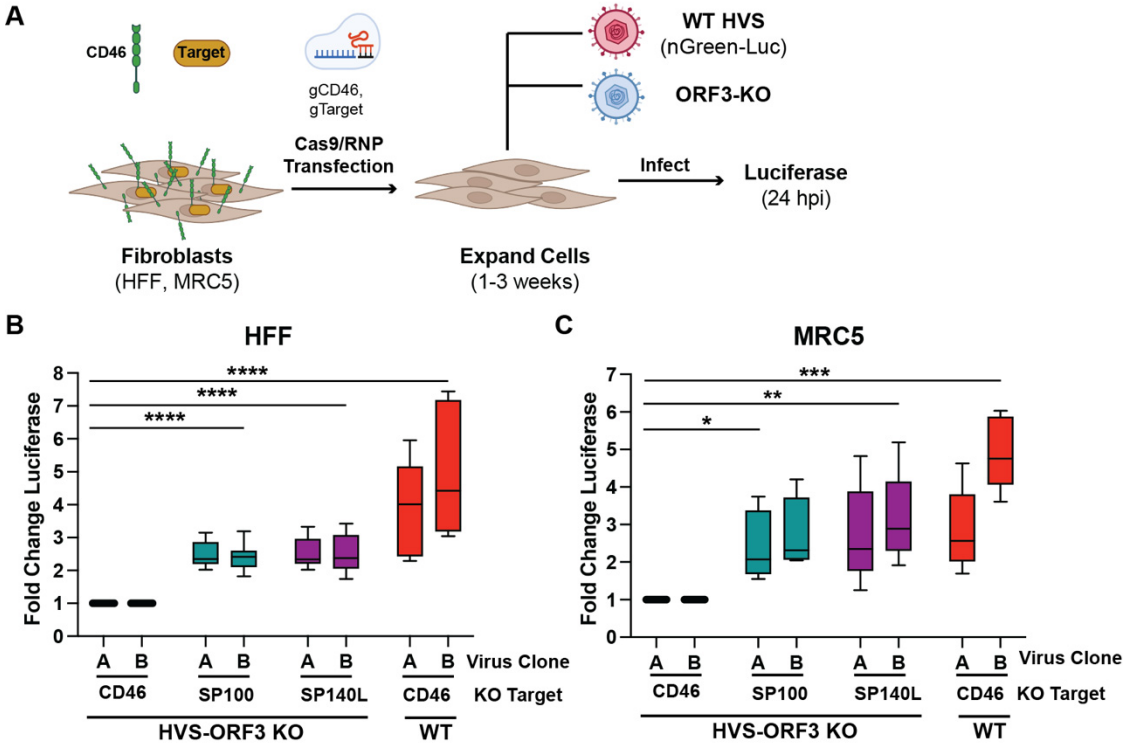

440
441 **Figure 7. Sp100 and Sp140L restrict Herpesvirus Saimiri (HVS) in the absence of ORF3.** (**A**).
442 Schematic of experiment. Fold change in luciferase expression HFF cells (n=7) (**B**) or MRC5 cells (n=5) (**C**)
443 infected with HVS-ORF3 Knockout or WT virus encoding luciferase with knockout of control *CD46*, *SP100*,
444 or *SP140L*. Two virus preparation (A and B) were used. P values calculated by Dunnett's multiple
445 comparisons test using an ordinary two-way ANOVA. * Indicates p-values <0.05, ** indicates p-values <0.01,
446 **** indicates p value < 0.0001.

447 **Discussion**

448 Herpesviruses infect nearly all animal species and result in lifelong latent and
449 persistent infections[69]. As DNA viruses, herpesviruses must overcome cellular barriers to
450 establish infection, including the detection and chromatinization of their foreign DNA
451 genomes by intrinsic restriction factors such as those in PML-NBs, including Sp100. Here,
452 we have identified Sp140L, an Sp100-homolog, as a novel restriction factor of herpesvirus
453 infection that is counteracted by the EBV latency protein EBNA-LP and the HVS tegument
454 protein ORF3. Our data are consistent with a mechanistic model whereby both Sp100
455 and Sp140L restrict EBV infection by preventing the expression of the essential viral
456 latency genes that are expressed after EBNA-LP and EBNA2, and by altering cellular
457 gene expression - both inducing an ISG response and reducing B cell metabolic capacity.
458 While the core antiviral PML-NB proteins have been thought to include PML, Sp100,
459 DAXX, and ATRX, our work adds the evolutionarily recent Sp140L to the list of key cellular
460 intrinsic restriction factors of DNA viruses in primates.

461 Leveraging a targeted CRISPR screen, we identified Sp100 and Sp140L as key
462 restriction factors that prevent EBV transformation of naïve B cells in the absence of
463 EBNA-LP and viral transcription of HVS in the absence of ORF3. Since knocking out other
464 PML-NB components did not rescue LPKO EBV, these other components of PML-NBs
465 must either be fully targeted by other EBV proteins, exhibit functional redundancy, or are
466 not required to block EBV-mediated transformation. Based on studies of HSV and CMV
467 mutants that lack abilities to inhibit PML-NB functions[13,30,32,70,71], we can conclude that
468 PML-NBs have two parallel repressive pathways in humans: one driven by DAXX/ATRX
469 and another by Sp100 and – we now propose – Sp140L. In the LPKO virus, its DAXX-
470 counteracting tegument protein BNRF1 is still intact, suggesting that factors in our screen
471 that failed to rescue naïve B cell transformation may be part of the DAXX-associated
472 pathway. While DAXX/ATRX load repressive histones (e.g. H3.3) onto the incoming viral
473 genome[13], Sp100 and Sp140L may be responsible for the addition of repressive histone
474 marks such as H3K9me3 and/or H3K27me3. For example, during latent KSHV infection
475 of endothelial cells, loss of Sp100, but not DAXX nor PML, correlates with H3K27me3
476 deposition on the viral genome[72], although Sp100's ability to bind heterochromatin protein

477 1 (HP1) and high-mobility group protein B1 (HMGB2)[73] suggests Sp100 may also be
478 linked to H3K9me3[74].
479 While PML-NB components are known to restrict DNA virus gene expression, we
480 discovered that Sp100 and Sp140L are also important in suppressing cellular proliferation.
481 Possible mechanisms of restricting proliferation include the failure to express the LMPs
482 during LPKO infection, however, LMP1 is not essential for the initial cell divisions after
483 EBV infection[75]. An alternative mechanism explaining these results is that these factors
484 integrate intrinsic DNA sensing with an anti-proliferative ISG response. Recent evidence
485 suggests Sp100 can localize to ISG promoters[10] suggesting Sp100 – and perhaps by
486 extension Sp140L – induce ISGs through direction transcriptional regulation or chromatin
487 modification at ISG promoters - as has been observed with other PML-NB components
488 including HIRA[7,8], ATRX[9], and PML[11] in mutant HSV- and HCMV-infected cells or upon
489 IFN stimulation. We also observed a restoration of expression of proliferation-linked
490 genes upon knockout of *SP100* or – more convincingly – *SP140L*, suggesting that
491 detection of foreign DNA or upregulation of ISG proteins may repress pro-proliferative
492 genes. For example, RSAD2, an ISG highly expressed during LPKO compared to WT
493 EBV infection, influences cellular metabolism and mitochondrial function[76,77]. IRF proteins
494 can also target metabolic genes [78,79], and notably several IRFs were also identified as
495 potential mediators of gene changes in LPKO-infected cells by ChEA3 (**Figure 3G and**
496 **3H**). In contrast, whether Sp100 and Sp140L impose cellular arrest by functioning as cell
497 cycle checkpoint proteins, therefore resulting in loss of proliferation-associated genes
498 remains unknown. Still, these findings suggest Sp100 and Sp140L impose an antiviral
499 state through not only regulating key viral genes, but also through repression of cell cycle
500 progression to impose an anti-proliferative state not favorable for viral infection or
501 transformation.
502 To further investigate the mechanism by which EBNA-LP may disrupt Sp100 and
503 Sp140L, we used AlphaFold3 to generate the first predicted structure of EBNA-LP and
504 found that an alpha helix in the C-terminal Y domain of EBNA-LP is predicted to associate
505 with the CARD domain of Sp100 and Sp140L. Mutagenesis of the leucine-rich motif
506 (LXXXLL) within this alpha helix reduces the ability of EBNA-LP to trans-complement the
507 LPKO virus in the transformation of naïve B cells. Our previous work identified this motif

508 as important for EBNA-LP to associate with the cellular transcription factor YY1[53]. This
509 motif is similar in sequence to both the LXXLL motif found in many cellular proteins that
510 regulate transcription[80], and to a similar but more diverse in sequence motif termed
511 "flexiNR" that is encoded in many viral proteins with transcription regulation functions[81].
512 Our findings fit with the notion that many viral proteins, including viral oncoproteins, have
513 evolved short linear motifs, generally less than 10 residues long in which a few key
514 residues define affinity and specificity, in order to mimic and/or hijack cellular protein
515 functions[82,83]. One such example includes the LXCXE motif in the many viral proteins that
516 can promote S Phase transition through interaction with pRb, p107, and p130[84]. Therefore,
517 this LXXXLL motif is an example of short linear motif critical for viral protein function.
518 This study was strengthened by the use of primary cells rather than cancer cell
519 lines. This is critical as PML-NBs functions can be disrupted in cancer cells, and therefore
520 the use of cancer cell lines for DNA sensing or virus restriction assay may not reflect
521 physiological relevance[8]. Still, there are limitations to performing knockouts in primary B
522 cells, as to reduce cell death prior to infection, B cells are infected with EBV only 2 hours
523 post-transfection. Therefore, as EBNA-LP is one of the earliest expressed EBV latency
524 proteins, turnover of targeted protein may be incomplete by the time EBNA-LP would be
525 expressed, even if genomic editing has occurred, and therefore this assay cannot fully
526 complement the LPKO virus. While the HVS assay using primary fibroblasts to generate
527 knockout cell lines prior to infection does not have the same temporal disadvantage, it
528 was challenging to get complete knockout of target genes even in cells with the proxy
529 target, CD46, lost. While overcoming these limitation would likely allow for an even more
530 pronounced rescue of the LPKO and ORF3-KO viruses with knockout of *SP100* and
531 *SP140L*, our assays clearly show that both *SP100* and *SP140L* restrict these diverse
532 herpesviruses. Furthermore, in our assays, knockout of *SP140L* resulted in stronger
533 phenotypic rescue – supporting Sp140L as the predominant speckled protein restricting
534 DNA viruses. However, we cannot exclude the possibility these observations are a result
535 of differences in knockout efficiency between *SP100* and *SP140L*.
536 The *SP140L* gene was formed by a gene duplication and cross-over event
537 between *SP100* and *SP140* shortly prior to the emergence of primates[29]. As a result, the
538 Sp140L N-terminal CARD domain is over 90% identical to that of Sp100, while its C-

539 terminal SAND and PHD/Bromodomains are very like those of Sp140[29]. Sp140L also
540 lacks the exons that in Sp100 encode SUMOylation and HP1 binding motifs but retains
541 the exons that in Sp100 can bind to the high mobility group protein HMGB2. Given the
542 CARD domain is responsible for the dimerization[24,85] or multimerization[86] of Sp100 and
543 that Sp100 and Sp140L colocalize in cells[29], and that Sp100 can form homotypic
544 interactions with the more distantly related protein Sp110[87], we anticipate that Sp100 and
545 Sp140L can interact, perhaps interchangeably, through this domain. This is further
546 supported by our findings that knockout of either Sp100 or Sp140L alone was sufficient
547 for rescue of transformation. Whether Sp140L arose as the result of an evolutionary arms
548 race with viral antagonists of Sp100 remains a possibility. As knockout of Sp140 did not
549 enhance transformation of either WT- or LPKO-infected B cells, further analysis of the
550 molecular differences between Sp140L and Sp140 – and the key domains responsible
551 for DNA virus restriction requires further investigation. Additionally, expression differences
552 between Sp100 and Sp140L may contribute to the dependency of EBNA-LP in naïve, but
553 not memory B cell transformation as at the RNA level, naïve B cells more highly express
554 both Sp100 and Sp140L[88].

555 Based on what is known about Sp100, we can propose the following model for
556 how both Sp100 and Sp140L might sense and suppress incoming viral genomes. The
557 SAND domain of Sp100 is reported to preferentially bind pairs of unmethylated CpG
558 dinucleotides[89]. Its PHD/Bromodomain contains bulky residues where other
559 PHD/Bromodomains contain binding pockets for histone modifications[90]. CARD domains
560 commonly multimerize through homotypic interactions to activate immune signaling
561 pathways[91]. Speckled proteins Sp100, Sp110[87], and Sp140[92,93] also associate on cellular
562 chromatin at gene promoters including Sp100A at ISGs[10], with Sp140 localizing to sites
563 enriched in H3K27me3 to maintain heterochromatin[92,93]. We hypothesize therefore that
564 the SAND domain of Sp100 (and by extension Sp140L) recognize the unmethylated
565 incoming viral DNA as foreign, perhaps in combination with the PHD/Bromodomain
566 recognizing features of newly assembled chromatin. Multimerization of Sp100 and
567 Sp140L proteins along the viral genome can then block the initiation of transcription of
568 viral genes (with only immediate early genes having escaped repression) either directly
569 or by recruiting repressors like HP1 or other chromatin remodeling factors to promote or

570 maintain the viral genome heterochromatin. Meanwhile, viral infection may also influence
571 Sp100 and/or Sp140L localization to cellular gene promoters, perhaps relieving
572 repressive epigenetic marks at the loci of ISGs. Alternatively, multimerization of the CARD
573 domains nucleates a signaling process that activates transcription of ISGs[87], activating
574 cell division checkpoints to suppress proliferation of a cell that has potentially been
575 invaded by a persistent foreign genome.
576 In conclusion, we identify Sp140L as a restriction factor of herpesviruses, and likely
577 all DNA viruses, targeted by critical viral proteins of primate viruses, but may represent a
578 significant barrier to any virus with a nuclear DNA phase of its lifecycle that transmits from
579 non-primate mammals. Not only does Sp140L restrict viral infection by preventing the
580 transcription of key viral genes, but also by promoting an ISG response that suppresses
581 cellular pro-proliferative pathways, and curbs the metabolic remodeling required for
582 cellular transformation that is a feature of persistent virus infections.
583

584 **Acknowledgements**

585 This work was supported by NIH Grant R01CA140337 (to M.A.L), MRC grant
586 MR/L008432/1 (to R.E.W.), and F31DE031509 (to J.M.C.). We acknowledge Ashely P.
587 Barry for reagent generation and technical assistance with the SeahorseXF assay, Elliott
588 SoRelle for assistance with scRNAseq analysis, Gillian Horn for assistance with flow
589 cytometry panels, Neha Shaw for technical assistance, Michael di Franco for pilot HVS
590 experiments, Johanna Veldman for historic Sp140L experiments, and Nicolás Reinoso-
591 Vizcaino for helpful discussions. We wish to thank the Duke University School of Medicine
592 Sequencing and Genomic Technologies Shared Resource for sequencing services and
593 the Duke Cancer Institute Flow Cytometry Facility for instrumentation.
594

595 **Resource Availability**

596 All sequencing data is publicly available from the NCBI's Gene Expression Omnibus
597 (GEO) under accession numbers: GSE282376, GSE282377, and GSE282400.
598

599 **Author contributions**

600 Conceptualization - M.A.L., R.E.W., J.M.C.

601 Methodology - J.M.C., W.W., R.E.W., M.A.L.
602 Investigation - J.M.C., W.W., J.G.
603 Formal Analysis - J.M.C., W.W., J.G., M.A.L.
604 Writing – Original Draft – J.M.C.
605 Writing – Review and Editing – J.M.C, M.A.L, R.E.W.,
606 Visualization - J.M.C., W.W., J.G., M.A.L, R.E.W.
607 Supervision - M.A.L, R.E.W.
608 Funding Acquisition - M.A.L, R.E.W, J.M.C.
609

610 **Declarations of Interests**

611 The authors declare no competing interests.
612

613 **Supplemental Information**

614 Document S1. Figures S1-S7
615 Table S1.
616
617

618 **STAR Methods**

619 **EBV Virus Preparation**

620 WT and LPKO viruses were prepared from 293-EBV producer lines and Raji Green Unit
621 titer was obtained as previously described[44]. In brief, LPKO virus refers to LPKO^{w} from
622 Szymula et al.[44] which contains a stop codon in exon W2 of every internal W repeat and
623 WT EBV refers to WT^{w} which contains a repaired stop codon in one W repeat found in
624 the parental B95-8 virus that (unlike B95-8) allows robust EBNA-LP expression[94].

625 **PBMC Isolation and Total/Naïve B and Pan B Cell Enrichment**

626 Adult buffy coats were obtained from the Gulf Coast Regional Blood Center
627 (Pro00006262) and Cord Blood was obtained from the Carolinas Cord Blood Bank
628 (Pro00061264) PBMCs were isolated as previously described [53]. Total B cells were
629 isolated using the EasySep Human Pan-B Cell Enrichment kit (STEMCELL Technologies
630 #19554) or MojoSort Human Pan B Isolation kit (Biolegend # 480082). To obtain isolated

631 naïve and memory B cells for SeahorseXF, the EasySep Human Memory B Cell Isolation
632 kit (STEMCELL Technologies #17864) was used. And, to isolate only naïve B cells for the
633 knockout screen and RNA-sequencing, the EasySep Human Naïve B cell isolation kit was
634 used (STEMCELL Technologies, #17254). Purity of isolated cells was assessed by flow
635 cytometry using antibodies to CD19, CD27, and IgD.

636 **EBV Infection**

637 Isolated B cells were infected by adding WT or LPKO virus at a ratio of 0.2 Raji Green
638 Units per cell and incubating at 37°C for 1 hour. Following incubation, cells were pelleted
639 and resuspended in Roswell Park Memorial Institute (RPMI) medium 1640 supplemented
640 with 20% heat-inactivated fetal bovine serum (FBS) (Corning) (R20 media) at
641 approximately 3 million cells/mL.

642 **Collection of scRNAseq samples, library preparation, sequencing, and processing**

643 Samples were viably frozen at each time point in 90% FBS + 10% DMSO and stored in
644 liquid N_2. Cryopreserved samples were then thawed simultaneously and enriched for
645 viable cells by Ficoll gradient. Libraries from 10,000 cells were then prepared in house
646 using the 10x Chromium GEM-X Single Cell 3' Gene Expression kit (10x
647 Genomics,1000691). Libraries were pooled and sequenced by the Duke Sequencing and
648 Genomic Technologies core facility on the NovaSeq 6000 S2 at 50 base pair read depth,
649 with paired end reads. Reads were mapped to the human genome and type 1 EBV
650 genome as previously described[54].

651 **scRNAseq QC Filtering and Analysis**

652 scRNAseq analysis was performed in R using package Seurat[95]. QC filtering and
653 clustering of samples into subpopulations was performed as previously described[54]. To
654 identify the biological features of each cluster, gene ontology analysis was performed
655 using clusterProfiler[96] and the top 100 genes differentially expressed in the previously
656 identified B95-8 subpopulations[54] were compiled and used to add module scores for each
657 subpopulation to the clusters identified in this experiment.

658 **Flow Cytometry**

659 For analysis of B cell isolation purity (CD19, Biolegend, 302212) and CD23 upregulation
660 (Biolegend, 338516), naïve B cells isolation purity (IgD Biolgened, 348210, CD27
661 Biolegend 302824), CD46 knockout efficiency (Biolgened, 352405), and ICAM1
662 expression (Biolegend, 353116) flow cytometry was performed on the BD FACSCanto II
663 (BD Biosciences) and samples were prepared as previously described[53]. When
664 quantifying outgrowth of CD46 negative cells, the high throughput sampler was used to
665 collect precise sample volumes.

666 Flow cytometry was also performed to validate the scRNA-sequencing data using the
667 identified markers using spectral flow cytometry on a Cytek Aurora (Cytek Biosciences).
668 Isolated Pan B cells were stained with CellTraceViolet (ThermoFisher, MPK1096) at 0.1
669 μM in PBS for 20 minutes at 37°C with gentle mixing every 5 minutes. Staining was then
670 quenched by adding 4x volume of R20 media and incubating for 5 minutes at 37°C. An
671 aliquot of cells was also infected that were not stained with CellTraceViolet to use as a
672 staining control. After pelleting, cells were infected with virus. At each time point collected,
673 cells were first washed in PBS and stained with LiveDead Blue (ThermoFisher, L23105)
674 for 20 minutes in the dark. Samples were then washed with FACS buffer (PBS + 2% FBS)
675 and stained with antibodies as above (CCR6 Invitrogen, 12-1969-42, CD23 Biolegend,
676 338516, ICAM1 Biolegend 353114, CD38 Biolegend 303529). Unstained cells were used
677 for reference controls for unmixing at each time point, along with single stained
678 compensation beads (BD Biosciences, 552843). To ensure accurate staining and analysis,
679 fluorescence minus one controls, isotype controls, and single stained samples were also
680 prepared for each time point. All flow cytometry data was analyzed in FlowJo (FlowJo,
681 LLC).

682 **SeahorseXF Assay**

683 Four days post infection, naïve and memory infected B cells were collected. Using flow
684 cytometry, CD19 and CD23 expression was assessed to ensure comparable infectivity
685 between WT and LPKO.

686 One day prior to the assay, the XFe96 sensor cartridge was submerged in tissue culture
687 grade water overnight at 37°C in a non-CO_2 incubator, along with XF calibrant (Agilent,
688 100840-00). The following day, the sensor cartridge was then placed in a utility plate

689 containing the pre-warmed XF Calibrant for 1 hour in the non-CO_2 incubator before
690 running the assay.

691 A 96-well Seahorse XF plate was coated with poly-D-lysine to keep suspension cells
692 adhered to the bottom of the wells. Cells were then harvested to the plate at 250,000 cells
693 per well in 50 µL XF Base Medium (RPMI supplemented with 10 mM glucose, 1 mM
694 sodium pyruvate, and 2 mM L-glutamine) (Agilent, 103681-100) and adhered to the plate
695 by briefly centrifugation. 130 µL warm assay media was then added to each well and
696 placed in the non-CO_2, 37°C incubator for 1 hour.

697 The XF Real-time APT Rate Assay was used (Agilent, 103592-100). Ports were loaded
698 with oligomycin and Rotenone/Antimycin A at working concentrations of 1.5 µM and 0.5
699 µM respectively. The calibrated sensor was then placed in the plate and the assay was
700 then run on the Seahorse XF Pro Analyzer (Agilent).

701 **Bulk RNASeq Sample Collection**

702 RNAseq libraries were prepared from samples 8 days post infection. Pan B cells from
703 three donors total were isolated, however, due to low yield, two of the three donors were
704 pooled together at the time of infection for a total of two Pan B pools infected with
705 separately with WT and LPKO virus. A Ficoll gradient was used to remove dead cells from
706 the harvested samples.

707 RNA-seq libraries were also prepared 5 days post infection for two donors in which naïve
708 B cells were isolated, transfected with guides targeting CD46, CD46 and SP100, or CD46
709 and SP140L prior to infection with LPKO or WT virus. Due to low cell counts, cells were
710 not sorted and therefore contain a mixed population of CD46 negative and positive cells
711 (**Figure S6A**), although the majority of cells were CD46 negative.

712 **Bulk RNASeq Library Preparation and Analysis**

713 RNA was isolated using the Qiagen RNeasy mini extraction kit including on-column
714 DNase digestion (74104). Libraries were prepared using the NEBNext Ultra II RNA Library
715 Prep kit (E770S) and sequenced as previously described[53]. QC of prepared libraries was
716 assessed using a TapeStation (Agilent). Reads were aligned to hg38 (Day 8 bulk RNAseq

717 samples) or hg38 with the Type 1 EBV genome (Day 5 knockout RNAseq samples) using
718 Hisat2. Samtools was then used to generate bam files. DESeq2 was used to generate a
719 ranked list of differentially expressed genes for Gene Set Enrichment Analysis (GSEA)[97].

720 **Knockout Screen in EBV Infected Naïve B Cells**

721 Following naïve B cell isolation as described above, cells rested overnight in R20 at 37°C.
722 For transfection, Cas9/RNP complexes were prepared and cells were washed and
723 resuspended in Buffer T (Neon Transfection System) as previously described[53]. 400,000
724 cells were transfected with Cas9/RNP complexes using the ThermoFisher Neon
725 Transfection System at 2150 V, 20 ms, 1 pulse and resuspended in 200 µL R20 in a 96
726 well V-bottom plate and incubated at 37°C. One hour after transfection, cells were infected
727 with WT or LPKO virus as described above. Following infection and removal of virus, cells
728 were resuspended in 200 µL R20 and moved to a flat bottom 96 well plate.

729 Precise sample volumes were used for flow cytometry at each time point to calculate total
730 cell numbers. Two days post infection, cells were stained with anti-CD19 (Biolegend,
731 302212) to quantify total number of cells per well for normalization. 7-, 14-, 21-, and 28-
732 days post infection, samples were stained with anti-CD46 (Biolegend, 352409) to quantify
733 outgrowth of edited cells. As infected cells expanded, fresh R20 was added in precise
734 volumes to maintain optimal cell density and allow for calculation of total cells per sample.
735 Generation of LCLs was determined by observations including cell clumping and media
736 color change indicative of proliferation and ability to passage or expand cells *in vitro*.

737 **Trans-complementation Assay**

738 This assay was performed as described previously[53]. Following PBMC isolation, cord
739 blood B cells were isolated by Pan B cell isolation (STEMCELL Technologies #19554).
740 Isolated cells were transfected with the trans-complementation plasmid (ori-P based
741 episomal plasmid in backbone pCEP4) prior to infection with LPKO or WT virus. The
742 trans-complementation plasmid encoded tdTomato followed by a P2A cleavage site, and
743 either empty vector, wild type EBNA-LP, or mutant EBNA-LP in which the Y domain
744 leucines (Leu276, Leu780, and Leu781), of the sequence LXXXLL were modified to
745 alanine by site-directed mutagenesis (Agilent, 200521). Outgrowth of tdTomato positive

746 cells was assess by flow cytometry each week until 35 days post-infection, with
747 compensation for the viral-encoded GFP. At this final timepoint, wells were considered
748 transformed into tdTomato positive LCLs if cells were both tdTomato-expressing and
749 contained proliferating cells passaged in culture.

750 **Prediction of Protein Structure by AlphaFold3**

751 Protein structures were predicting using the AlphaFold server
752 (https://alphafoldserver.com) using default settings. To predict the structure of a single
753 molecular of EBNA-LP, the sequence of wild type EBNA-LP (UniProt Q8AZK7) encoding
754 4 W domains was used for input, and the representative model 0 was selected for
755 visualization using PyMOL[98]. For EBNA-LP/Sp140L (UniProt Q9H930) and EBNA-
756 LP/Sp100 (UniProt P23497) complexes, jobs were submitted with 2 molecules of each
757 protein. Model 0 for each complex was representative of predicted models and selected
758 for visualization. For complexes containing SP140L, isoform 2, which excludes the
759 frequently skipped exon 2[29], was used. For Sp100, the Sp100C isoform was used as it
760 contains the most similar domain architecture to Sp140L.

761 **Generation of Recombinant HVS Virus**

762 A BAC clone of the HVS A11-Sac strain (which lacks the HVS transforming genes)[99]
763 was modified using RecA-mediated recombineering to replace the AgeI-BlpI fragment of
764 dsRed1 ORF with a mNeonGreen-T2A-Luciferase fusion. This generated two BAC
765 clones (A and B) that were each recombineered to delete the ORF3 open reading
766 frame, introducing a STOP codon (alongside SalI and Cla I restriction sites) after the 5th
767 amino acid of ORF3, and deleting all but the last 237 nucleotides of the ORF3 coding
768 sequence, thereby generating two independent HVS-ORF3KO BACs (A-ORF3 KO and
769 B-ORF3 KO) (as validated in **Figure S7A**).
770

771 **HVS Virus Preparation**

772 Herpesvirus saimiri BAC is transfected into – using a peptide-lipofectin complex[100] – or
773 inoculated onto Owl Monkey kidney (OMK) cells. Supernatant is harvested when the
774 cell monolayer is largely destroyed (typically after 4-7 days), and centrifuged to remove
775 cell debris.

776

777 **HVS Genome Quantification**

778 Virus stock was lysed by lysis buffer after DNase treatment. Then virus lysate was
779 subjected to quantify viral DNA by using Kapa SYBR Fast Universal qPCR kit (KK4602,
780 SLS) with a pair of hygromycin gene primer.

781

782 **Generation of *CD46*, *SP100*, and *SP140L* Knockout Fibroblast Cell Lines**

783 Human Foreskin Fibroblasts (HFF) and human lung fibroblast cell line MRC-5 (MRC5)
784 were maintained in Dulbecco's modified Eagle's medium (DMEM) (Gibco, Grand Island,
785 NY, USA) supplemented with 10% heat-inactivated fetal bovine serum (Gibco, Grand
786 Island, NY, USA) at 37°C in a 5% CO2. For transfection, Cas9/RNP complexes were
787 prepared in buffer T whereas cells were washed and resuspended in buffer R (Neon
788 transfection system). $2x10^5$ cells in 5 ul buffer R were mixed with Cas9/RNP complexes
789 and transfected with the neon transfection system at 1650 V 10 ms, 3 pulses. Then the
790 transfected cells were resuspended in 300 µl of 15% DMEM in 12 well plate and
791 incubated at 37°C. When cell confluency reached 80-90%, a quarter of the well was
792 stained with anti-CD46 antibody (Biolegend, 352401) to measure CD46-knockout
793 efficiency by flow cytometry as described above.

794

795 **Immunofluorescence in Fibroblast Knockout Lines**

796 HFF cells were seeded onto coverslips. At 24 hours post HVS infection, the coverslips
797 were fixed with 4% PFA for 15 minutes and permeabilized with 0.5% Triton X-100 in PBS
798 for 15 minutes. Coverslips were blocked with 10% FBS in PBS for 1 hour. The coverslips
799 were incubated with the anti-Sp100 (Invitrogen, PA5-78177) for 1 hour followed by Alexa
800 Fluor 546 conjugated anti-rabbit IgG (Invitrogen, A11071) for 1 hour. The coverslips were
801 mounted with ProLong® Gold Antifade Reagent with DAPI (Cell Signaling Technology,
802 8961). Images were obtained using the EVOS cell imaging system.

803

804 **Knockout Screen in HVS Infected Fibroblast Cell Lines**

805 Fibroblast cells were seeded 100 ul of $3x10^5$ cells/ml triplicate wells of a white 96 well
806 clear-bottom plate. HVS WT (A and B) and HVS ORF3 KO (A-ORF3 and B-ORF3) were

807 used to infect knockout cell line at MOI of 1000 genomes/ml. After 24 hours, luciferase
808 activity was measured as a proxy for HVS transcription: cell media was removed and
809 replaced with 50 µl fresh media, to which 50 µl Steady-Glo® Luciferase Assay System
810 reagent (Promega, E2510) was added, and after 5 minutes, luminescence was
811 measured on a FluoStar OMEGA plate reader (BMG Labtech).
812
813 **Knockout Validation**
814 Knockout cell lines were validated by genomic DNA (gDNA) sequencing at targeted cut
815 sites. For LPKO LCLs, the total population of LCLs (regardless of CD46 expression) was
816 used to collect samples for gDNA – as if targets have the ability to rescue LPKO infection,
817 we expect that all surviving cells are edited. Cells were pelleted and washed in PBS.
818 gDNA was isolated (K182002, ThermoFisher) and primers spanning cut sites were used
819 to amplify region of interest. gDNA from control (CD46 only) conditions were used for
820 comparison. PCR product was sequenced, and the Synthego ICE Analysis tool was used
821 to generate a knockout score (frequency of cells containing knockout).
822
823 **Western Blotting**
824 Western blots were performed as previously described[53].
825
826 **REFERENCES**

827 1. Cohen, J.I. (2020). Herpesvirus latency. J Clin Invest *130*, 3361-3369.
828 10.1172/JCI136225.
829 2. Lanz, T.V., Brewer, R.C., Ho, P.P., Moon, J.S., Jude, K.M., Fernandez, D.,
830 Fernandes, R.A., Gomez, A.M., Nadj, G.S., Bartley, C.M., et al. (2022). Clonally
831 expanded B cells in multiple sclerosis bind EBV EBNA1 and GlialCAM. Nature
832 *603*, 321-327. 10.1038/s41586-022-04432-7.
833 3. Bjornevik, K., Cortese, M., Healy, B.C., Kuhle, J., Mina, M.J., Leng, Y., Elledge,
834 S.J., Niebuhr, D.W., Scher, A.I., Munger, K.L., and Ascherio, A. (2022).
835 Longitudinal analysis reveals high prevalence of Epstein-Barr virus associated
836 with multiple sclerosis. Science *375*, 296-301. 10.1126/science.abj8222.
837 4. Wong, Y., Meehan, M.T., Burrows, S.R., Doolan, D.L., and Miles, J.J. (2022).
838 Estimating the global burden of Epstein-Barr virus-related cancers. J Cancer Res
839 Clin Oncol *148*, 31-46. 10.1007/s00432-021-03824-y.
840 5. Corpet, A., Kleijwegt, C., Roubille, S., Juillard, F., Jacquet, K., Texier, P., and
841 Lomonte, P. (2020). PML nuclear bodies and chromatin dynamics: catch me if
842 you can! Nucleic Acids Res *48*, 11890-11912. 10.1093/nar/gkaa828.

843 6. Roy, A., and Ghosh, A. (2024). Epigenetic Restriction Factors (eRFs) in Virus
844 Infection. Viruses *16*. 10.3390/v16020183.
845 7. Kleijwegt, C., Bressac, F., Seurre, C., Bouchereau, W., Cohen, C., Texier, P.,
846 Simonet, T., Schaeffer, L., Lomonte, P., and Corpet, A. (2023). Interplay between
847 PML NBs and HIRA for H3.3 dynamics following type I interferon stimulus. Elife
848 *12*. 10.7554/eLife.80156.
849 8. McFarlane, S., Orr, A., Roberts, A.P.E., Conn, K.L., Iliev, V., Loney, C., da Silva
850 Filipe, A., Smollett, K., Gu, Q., Robertson, N., et al. (2019). The histone
851 chaperone HIRA promotes the induction of host innate immune defences in
852 response to HSV-1 infection. PLoS Pathog *15*, e1007667.
853 10.1371/journal.ppat.1007667.
854 9. Stilp, A.C., Scherer, M., Konig, P., Furstberger, A., Kestler, H.A., and Stamminger,
855 T. (2022). The chromatin remodeling protein ATRX positively regulates IRF3-
856 dependent type I interferon production and interferon-induced gene expression.
857 PLoS Pathog *18*, e1010748. 10.1371/journal.ppat.1010748.
858 10. Dong, H., Wu, W., Li, J., Ma, Y., Deng, X., Guo, D., and Xu, P. (2022). PML Body
859 Component Sp100A Is a Cytosolic Responder to IFN and Activator of Antiviral
860 ISGs. mBio *13*, e0204422. 10.1128/mbio.02044-22.
861 11. Kim, Y.E., and Ahn, J.H. (2015). Positive role of promyelocytic leukemia protein in
862 type I interferon response and its regulation by human cytomegalovirus. PLoS
863 Pathog *11*, e1004785. 10.1371/journal.ppat.1004785.
864 12. Alandijany, T., Roberts, A.P.E., Conn, K.L., Loney, C., McFarlane, S., Orr, A., and
865 Boutell, C. (2018). Distinct temporal roles for the promyelocytic leukaemia (PML)
866 protein in the sequential regulation of intracellular host immunity to HSV-1
867 infection. PLoS Pathog *14*, e1006769. 10.1371/journal.ppat.1006769.
868 13. Tsai, K., Chan, L., Gibeault, R., Conn, K., Dheekollu, J., Domsic, J., Marmorstein,
869 R., Schang, L.M., and Lieberman, P.M. (2014). Viral reprogramming of the Daxx
870 histone H3.3 chaperone during early Epstein-Barr virus infection. J Virol *88*,
871 14350-14363. 10.1128/JVI.01895-14.
872 14. Albright, E.R., and Kalejta, R.F. (2016). Canonical and Variant Forms of Histone
873 H3 Are Deposited onto the Human Cytomegalovirus Genome during Lytic and
874 Latent Infections. J Virol *90*, 10309-10320. 10.1128/JVI.01220-16.
875 15. Schreiner, S., Burck, C., Glass, M., Groitl, P., Wimmer, P., Kinkley, S., Mund, A.,
876 Everett, R.D., and Dobner, T. (2013). Control of human adenovirus type 5 gene
877 expression by cellular Daxx/ATRX chromatin-associated complexes. Nucleic
878 Acids Res *41*, 3532-3550. 10.1093/nar/gkt064.
879 16. Cabral, J.M., Oh, H.S., and Knipe, D.M. (2018). ATRX promotes maintenance of
880 herpes simplex virus heterochromatin during chromatin stress. Elife *7*.
881 10.7554/eLife.40228.
882 17. Rai, T.S., Glass, M., Cole, J.J., Rather, M.I., Marsden, M., Neilson, M., Brock, C.,
883 Humphreys, I.R., Everett, R.D., and Adams, P.D. (2017). Histone chaperone
884 HIRA deposits histone H3.3 onto foreign viral DNA and contributes to anti-viral
885 intrinsic immunity. Nucleic Acids Res *45*, 11673-11683. 10.1093/nar/gkx771.
886 18. Cohen, C., Corpet, A., Roubille, S., Maroui, M.A., Poccardi, N., Rousseau, A.,
887 Kleijwegt, C., Binda, O., Texier, P., Sawtell, N., et al. (2018). Promyelocytic
888 leukemia (PML) nuclear bodies (NBs) induce latent/quiescent HSV-1 genomes

889 chromatinization through a PML NB/Histone H3.3/H3.3 Chaperone Axis. PLoS
890 Pathog *14*, e1007313. 10.1371/journal.ppat.1007313.
891 19. Negorev, D.G., Vladimirova, O.V., and Maul, G.G. (2009). Differential functions of
892 interferon-upregulated Sp100 isoforms: herpes simplex virus type 1 promoter-
893 based immediate-early gene suppression and PML protection from ICP0-
894 mediated degradation. J Virol *83*, 5168-5180. 10.1128/JVI.02083-08.
895 20. Everett, R.D., Parada, C., Gripon, P., Sirma, H., and Orr, A. (2008). Replication of
896 ICP0-null mutant herpes simplex virus type 1 is restricted by both PML and
897 Sp100. J Virol *82*, 2661-2672. 10.1128/JVI.02308-07.
898 21. Kim, Y.E., Lee, J.H., Kim, E.T., Shin, H.J., Gu, S.Y., Seol, H.S., Ling, P.D., Lee,
899 C.H., and Ahn, J.H. (2011). Human cytomegalovirus infection causes degradation
900 of Sp100 proteins that suppress viral gene expression. J Virol *85*, 11928-11937.
901 10.1128/JVI.00758-11.
902 22. Habiger, C., Jager, G., Walter, M., Iftner, T., and Stubenrauch, F. (2016).
903 Interferon Kappa Inhibits Human Papillomavirus 31 Transcription by Inducing
904 Sp100 Proteins. J Virol *90*, 694-704. 10.1128/JVI.02137-15.
905 23. Berscheminski, J., Wimmer, P., Brun, J., Ip, W.H., Groitl, P., Horlacher, T., Jaffray,
906 E., Hay, R.T., Dobner, T., and Schreiner, S. (2014). Sp100 isoform-specific
907 regulation of human adenovirus 5 gene expression. J Virol *88*, 6076-6092.
908 10.1128/JVI.00469-14.
909 24. Seeler, J.S., Marchio, A., Sitterlin, D., Transy, C., and Dejean, A. (1998).
910 Interaction of SP100 with HP1 proteins: a link between the promyelocytic
911 leukemia-associated nuclear bodies and the chromatin compartment. Proc Natl
912 Acad Sci U S A *95*, 7316-7321. 10.1073/pnas.95.13.7316.
913 25. Fraschilla, I., and Jeffrey, K.L. (2020). The Speckled Protein (SP) Family:
914 Immunity's Chromatin Readers. Trends Immunol *41*, 572-585.
915 10.1016/j.it.2020.04.007.
916 26. Ji, D.X., Witt, K.C., Kotov, D.I., Margolis, S.R., Louie, A., Chevee, V., Chen, K.J.,
917 Gaidt, M.M., Dhaliwal, H.S., Lee, A.Y., et al. (2021). Role of the transcriptional
918 regulator SP140 in resistance to bacterial infections via repression of type I
919 interferons. Elife *10*. 10.7554/eLife.67290.
920 27. Leu, J.S., Chen, M.L., Chang, S.Y., Yu, S.L., Lin, C.W., Wang, H., Chen, W.C.,
921 Chang, C.H., Wang, J.Y., Lee, L.N., et al. (2017). SP110b Controls Host Immunity
922 and Susceptibility to Tuberculosis. Am J Respir Crit Care Med *195*, 369-382.
923 10.1164/rccm.201601-0103OC.
924 28. Nakamura, H., Hikichi, H., Seto, S., Hijikata, M., and Keicho, N. (2024).
925 Transcriptional regulators SP110 and SP140 modulate inflammatory response
926 genes in Mycobacterium tuberculosis-infected human macrophages. Microbiol
927 Spectr *12*, e0010124. 10.1128/spectrum.00101-24.
928 29. Saare, M., Hamarik, U., Venta, R., Panarina, M., Zucchelli, C., Pihlap, M., Remm,
929 A., Kisand, K., Toots, U., Moll, K., et al. (2015). SP140L, an Evolutionarily Recent
930 Member of the SP100 Family, Is an Autoantigen in Primary Biliary Cirrhosis. J
931 Immunol Res *2015*, 526518. 10.1155/2015/526518.
932 30. Lukashchuk, V., McFarlane, S., Everett, R.D., and Preston, C.M. (2008). Human
933 cytomegalovirus protein pp71 displaces the chromatin-associated factor ATRX

934 from nuclear domain 10 at early stages of infection. J Virol *82*, 12543-12554.
935 10.1128/JVI.01215-08.
936 31. Hwang, J., and Kalejta, R.F. (2009). Human cytomegalovirus protein pp71
937 induces Daxx SUMOylation. J Virol *83*, 6591-6598. 10.1128/JVI.02639-08.
938 32. Tsai, K., Thikmyanova, N., Wojcechowskyj, J.A., Delecluse, H.J., and Lieberman,
939 P.M. (2011). EBV tegument protein BNRF1 disrupts DAXX-ATRX to activate viral
940 early gene transcription. PLoS Pathog *7*, e1002376.
941 10.1371/journal.ppat.1002376.
942 33. Full, F., Jungnickl, D., Reuter, N., Bogner, E., Brulois, K., Scholz, B., Sturzl, M.,
943 Myoung, J., Jung, J.U., Stamminger, T., and Ensser, A. (2014). Kaposi's sarcoma
944 associated herpesvirus tegument protein ORF75 is essential for viral lytic
945 replication and plays a critical role in the antagonization of ND10-instituted
946 intrinsic immunity. PLoS Pathog *10*, e1003863. 10.1371/journal.ppat.1003863.
947 34. Full, F., Reuter, N., Zielke, K., Stamminger, T., and Ensser, A. (2012). Herpesvirus
948 saimiri antagonizes nuclear domain 10-instituted intrinsic immunity via an ORF3-
949 mediated selective degradation of cellular protein Sp100. J Virol *86*, 3541-3553.
950 10.1128/JVI.06992-11.
951 35. Chelbi-Alix, M.K., and de The, H. (1999). Herpes virus induced proteasome-
952 dependent degradation of the nuclear bodies-associated PML and Sp100
953 proteins. Oncogene *18*, 935-941. 10.1038/sj.onc.1202366.
954 36. Lukashchuk, V., and Everett, R.D. (2010). Regulation of ICP0-null mutant herpes
955 simplex virus type 1 infection by ND10 components ATRX and hDaxx. J Virol *84*,
956 4026-4040. 10.1128/JVI.02597-09.
957 37. Kang, H., Kim, E.T., Lee, H.R., Park, J.J., Go, Y.Y., Choi, C.Y., and Ahn, J.H.
958 (2006). Inhibition of SUMO-independent PML oligomerization by the human
959 cytomegalovirus IE1 protein. J Gen Virol *87*, 2181-2190. 10.1099/vir.0.81787-0.
960 38. Ling, P.D., Peng, R.S., Nakajima, A., Yu, J.H., Tan, J., Moses, S.M., Yang, W.H.,
961 Zhao, B., Kieff, E., Bloch, K.D., and Bloch, D.B. (2005). Mediation of Epstein-Barr
962 virus EBNA-LP transcriptional coactivation by Sp100. EMBO J *24*, 3565-3575.
963 10.1038/sj.emboj.7600820.
964 39. Echendu, C.W., and Ling, P.D. (2008). Regulation of Sp100A subnuclear
965 localization and transcriptional function by EBNA-LP and interferon. J Interferon
966 Cytokine Res *28*, 667-678. 10.1089/jir.2008.0023.
967 40. Lu, Y., Orr, A., and Everett, R.D. (2016). Stimulation of the Replication of ICP0-
968 Null Mutant Herpes Simplex Virus 1 and pp71-Deficient Human Cytomegalovirus
969 by Epstein-Barr Virus Tegument Protein BNRF1. J Virol *90*, 9664-9673.
970 10.1128/JVI.01224-16.
971 41. Everett, R.D., Bell, A.J., Lu, Y., and Orr, A. (2013). The replication defect of ICP0-
972 null mutant herpes simplex virus 1 can be largely complemented by the
973 combined activities of human cytomegalovirus proteins IE1 and pp71. J Virol *87*,
974 978-990. 10.1128/JVI.01103-12.
975 42. Lu, Y., and Everett, R.D. (2015). Analysis of the functional interchange between
976 the IE1 and pp71 proteins of human cytomegalovirus and ICP0 of herpes simplex
977 virus 1. J Virol *89*, 3062-3075. 10.1128/JVI.03480-14.
978 43. Negorev, D.G., Vladimirova, O.V., Ivanov, A., Rauscher, F., 3rd, and Maul, G.G.
979 (2006). Differential role of Sp100 isoforms in interferon-mediated repression of

980 herpes simplex virus type 1 immediate-early protein expression. J Virol *80*, 8019-
981 8029. 10.1128/JVI.02164-05.
982 44. Szymula, A., Palermo, R.D., Bayoumy, A., Groves, I.J., Ba Abdullah, M., Holder,
983 B., and White, R.E. (2018). Epstein-Barr virus nuclear antigen EBNA-LP is
984 essential for transforming naive B cells, and facilitates recruitment of transcription
985 factors to the viral genome. PLoS Pathog *14*, e1006890.
986 10.1371/journal.ppat.1006890.
987 45. Peng, Q., Wang, L., Qin, Z., Wang, J., Zheng, X., Wei, L., Zhang, X., Zhang, X.,
988 Liu, C., Li, Z., et al. (2020). Phase Separation of Epstein-Barr Virus EBNA2 and
989 Its Coactivator EBNALP Controls Gene Expression. J Virol *94*.
990 10.1128/JVI.01771-19.
991 46. Harada, S., and Kieff, E. (1997). Epstein-Barr virus nuclear protein LP stimulates
992 EBNA-2 acidic domain-mediated transcriptional activation. J Virol *71*, 6611-6618.
993 10.1128/JVI.71.9.6611-6618.1997.
994 47. McCann, E.M., Kelly, G.L., Rickinson, A.B., and Bell, A.I. (2001). Genetic analysis
995 of the Epstein-Barr virus-coded leader protein EBNA-LP as a co-activator of
996 EBNA2 function. J Gen Virol *82*, 3067-3079. 10.1099/0022-1317-82-12-3067.
997 48. Nitsche, F., Bell, A., and Rickinson, A. (1997). Epstein-Barr virus leader protein
998 enhances EBNA-2-mediated transactivation of latent membrane protein 1
999 expression: a role for the W1W2 repeat domain. J Virol *71*, 6619-6628.
1000 10.1128/JVI.71.9.6619-6628.1997.
1001 49. Peng, R., Moses, S.C., Tan, J., Kremmer, E., and Ling, P.D. (2005). The Epstein-
1002 Barr virus EBNA-LP protein preferentially coactivates EBNA2-mediated
1003 stimulation of latent membrane proteins expressed from the viral divergent
1004 promoter. J Virol *79*, 4492-4505. 10.1128/JVI.79.7.4492-4505.2005.
1005 50. Yokoyama, A., Tanaka, M., Matsuda, G., Kato, K., Kanamori, M., Kawasaki, H.,
1006 Hirano, H., Kitabayashi, I., Ohki, M., Hirai, K., and Kawaguchi, Y. (2001).
1007 Identification of major phosphorylation sites of Epstein-Barr virus nuclear antigen
1008 leader protein (EBNA-LP): ability of EBNA-LP to induce latent membrane protein
1009 1 cooperatively with EBNA-2 is regulated by phosphorylation. J Virol *75*, 5119-
1010 5128. 10.1128/JVI.75.11.5119-5128.2001.
1011 51. Portal, D., Zhao, B., Calderwood, M.A., Sommermann, T., Johannsen, E., and
1012 Kieff, E. (2011). EBV nuclear antigen EBNALP dismisses transcription repressors
1013 NCoR and RBPJ from enhancers and EBNA2 increases NCoR-deficient RBPJ
1014 DNA binding. Proc Natl Acad Sci U S A *108*, 7808-7813.
1015 10.1073/pnas.1104991108.
1016 52. Portal, D., Rosendorff, A., and Kieff, E. (2006). Epstein-Barr nuclear antigen
1017 leader protein coactivates transcription through interaction with histone
1018 deacetylase 4. Proc Natl Acad Sci U S A *103*, 19278-19283.
1019 10.1073/pnas.0609320103.
1020 53. Cable, J.M., Reinoso-Vizcaino, N.M., White, R.E., and Luftig, M.A. (2024).
1021 Epstein-Barr virus protein EBNA-LP engages YY1 through leucine-rich motifs to
1022 promote naive B cell transformation. PLoS Pathog *20*, e1011950.
1023 10.1371/journal.ppat.1011950.
1024 54. SoRelle, E.D., Dai, J., Reinoso-Vizcaino, N.M., Barry, A.P., Chan, C., and Luftig,
1025 M.A. (2022). Time-resolved transcriptomes reveal diverse B cell fate trajectories

in the early response to Epstein-Barr virus infection. Cell Rep *40*, 111286. 10.1016/j.celrep.2022.111286.

55. Nikitin, P.A., Yan, C.M., Forte, E., Bocedi, A., Tourigny, J.P., White, R.E., Allday, M.J., Patel, A., Dave, S.S., Kim, W., et al. (2010). An ATM/Chk2-mediated DNA damage-responsive signaling pathway suppresses Epstein-Barr virus transformation of primary human B cells. Cell Host Microbe *8*, 510-522. 10.1016/j.chom.2010.11.004.

56. McFadden, K., Hafez, A.Y., Kishton, R., Messinger, J.E., Nikitin, P.A., Rathmell, J.C., and Luftig, M.A. (2016). Metabolic stress is a barrier to Epstein-Barr virus-mediated B-cell immortalization. Proc Natl Acad Sci U S A *113*, E782-790. 10.1073/pnas.1517141113.

57. Beer, S., Wange, L.E., Zhang, X., Kuklik-Roos, C., Enard, W., Hammerschmidt, W., Scialdone, A., and Kempkes, B. (2022). EBNA2-EBF1 complexes promote MYC expression and metabolic processes driving S-phase progression of Epstein-Barr virus-infected B cells. Proc Natl Acad Sci U S A *119*, e2200512119. 10.1073/pnas.2200512119.

58. Nakagawa, R., and Calado, D.P. (2021). Positive Selection in the Light Zone of Germinal Centers. Front Immunol *12*, 661678. 10.3389/fimmu.2021.661678.

59. Playoust, E., Remark, R., Vivier, E., and Milpied, P. (2023). Germinal center-dependent and -independent immune responses of tumor-infiltrating B cells in human cancers. Cell Mol Immunol *20*, 1040-1050. 10.1038/s41423-023-01060-7.

60. Forte, E., and Luftig, M.A. (2009). MDM2-dependent inhibition of p53 is required for Epstein-Barr virus B-cell growth transformation and infected-cell survival. J Virol *83*, 2491-2499. 10.1128/JVI.01681-08.

61. Keenan, A.B., Torre, D., Lachmann, A., Leong, A.K., Wojciechowicz, M.L., Utti, V., Jagodnik, K.M., Kropiwnicki, E., Wang, Z., and Ma'ayan, A. (2019). ChEA3: transcription factor enrichment analysis by orthogonal omics integration. Nucleic Acids Res *47*, W212-W224. 10.1093/nar/gkz446.

62. Liao, J., Chen, Z., Chang, R., Yuan, T., Li, G., Zhu, C., Wen, J., Wei, Y., Huang, Z., Ding, Z., et al. (2023). CENPA functions as a transcriptional regulator to promote hepatocellular carcinoma progression via cooperating with YY1. Int J Biol Sci *19*, 5218-5232. 10.7150/ijbs.85656.

63. Patterson, D.G., Kania, A.K., Price, M.J., Rose, J.R., Scharer, C.D., and Boss, J.M. (2021). An IRF4-MYC-mTORC1 Integrated Pathway Controls Cell Growth and the Proliferative Capacity of Activated B Cells during B Cell Differentiation In Vivo. J Immunol *207*, 1798-1811. 10.4049/jimmunol.2100440.

64. Ma, Y., Walsh, M.J., Bernhardt, K., Ashbaugh, C.W., Trudeau, S.J., Ashbaugh, I.Y., Jiang, S., Jiang, C., Zhao, B., Root, D.E., et al. (2017). CRISPR/Cas9 Screens Reveal Epstein-Barr Virus-Transformed B Cell Host Dependency Factors. Cell Host Microbe *21*, 580-591 e587. 10.1016/j.chom.2017.04.005.

65. Li, P., Spolski, R., Liao, W., Wang, L., Murphy, T.L., Murphy, K.M., and Leonard, W.J. (2012). BATF-JUN is critical for IRF4-mediated transcription in T cells. Nature *490*, 543-546. 10.1038/nature11530.

66. Arnold, P.R., Wen, M., Zhang, L., Ying, Y., Xiao, X., Chu, X., Wang, G., Zhang, X., Mao, Z., Zhang, A., et al. (2022). Suppression of FOXP3 expression by the

1071 AP-1 family transcription factor BATF3 requires partnering with IRF4. Front
1072 Immunol *13*, 966364. 10.3389/fimmu.2022.966364.
1073 67. Akidil, E., Albanese, M., Buschle, A., Ruhle, A., Pich, D., Keppler, O.T., and
1074 Hammerschmidt, W. (2021). Highly efficient CRISPR-Cas9-mediated gene
1075 knockout in primary human B cells for functional genetic studies of Epstein-Barr
1076 virus infection. PLoS Pathog *17*, e1009117. 10.1371/journal.ppat.1009117.
1077 68. Abramson, J., Adler, J., Dunger, J., Evans, R., Green, T., Pritzel, A.,
1078 Ronneberger, O., Willmore, L., Ballard, A.J., Bambrick, J., et al. (2024). Accurate
1079 structure prediction of biomolecular interactions with AlphaFold 3. Nature *630*,
1080 493-500. 10.1038/s41586-024-07487-w.
1081 69. Whitley, R.J. (1996). Herpesviruses. In Medical Microbiology, S. Baron, ed.
1082 70. Hwang, J., and Kalejta, R.F. (2007). Proteasome-dependent, ubiquitin-
1083 independent degradation of Daxx by the viral pp71 protein in human
1084 cytomegalovirus-infected cells. Virology *367*, 334-338.
1085 10.1016/j.virol.2007.05.037.
1086 71. Saffert, R.T., and Kalejta, R.F. (2007). Human cytomegalovirus gene expression
1087 is silenced by Daxx-mediated intrinsic immune defense in model latent infections
1088 established in vitro. J Virol *81*, 9109-9120. 10.1128/JVI.00827-07.
1089 72. Gunther, T., Schreiner, S., Dobner, T., Tessmer, U., and Grundhoff, A. (2014).
1090 Influence of ND10 components on epigenetic determinants of early KSHV
1091 latency establishment. PLoS Pathog *10*, e1004274.
1092 10.1371/journal.ppat.1004274.
1093 73. Lehming, N., Le Saux, A., Schuller, J., and Ptashne, M. (1998). Chromatin
1094 components as part of a putative transcriptional repressing complex. Proc Natl
1095 Acad Sci U S A *95*, 7322-7326. 10.1073/pnas.95.13.7322.
1096 74. Lachner, M., O'Carroll, D., Rea, S., Mechtler, K., and Jenuwein, T. (2001).
1097 Methylation of histone H3 lysine 9 creates a binding site for HP1 proteins. Nature
1098 *410*, 116-120. 10.1038/35065132.
1099 75. Pich, D., Mrozek-Gorska, P., Bouvet, M., Sugimoto, A., Akidil, E., Grundhoff, A.,
1100 Hamperl, S., Ling, P.D., and Hammerschmidt, W. (2019). First Days in the Life of
1101 Naive Human B Lymphocytes Infected with Epstein-Barr Virus. mBio *10*.
1102 10.1128/mBio.01723-19.
1103 76. Chen, S., Ye, J., Lin, Y., Chen, W., Huang, S., Yang, Q., Qian, H., Gao, S., and
1104 Hua, C. (2024). Crucial Roles of RSAD2/viperin in Immunomodulation,
1105 Mitochondrial Metabolism and Autoimmune Diseases. Inflammation.
1106 10.1007/s10753-024-02076-5.
1107 77. Honarmand Ebrahimi, K., Vowles, J., Browne, C., McCullagh, J., and James,
1108 W.S. (2020). ddhCTP produced by the radical-SAM activity of RSAD2 (viperin)
1109 inhibits the NAD(+) -dependent activity of enzymes to modulate metabolism.
1110 FEBS Lett *594*, 1631-1644. 10.1002/1873-3468.13778.
1111 78. Dinasarapu, A.R., Gupta, S., Ram Maurya, M., Fahy, E., Min, J., Sud, M.,
1112 Gersten, M.J., Glass, C.K., and Subramaniam, S. (2013). A combined omics
1113 study on activated macrophages--enhanced role of STATs in apoptosis, immunity
1114 and lipid metabolism. Bioinformatics *29*, 2735-2743.
1115 10.1093/bioinformatics/btt469.

1116 79. Hedl, M., Yan, J., and Abraham, C. (2016). IRF5 and IRF5 Disease-Risk Variants
1117 Increase Glycolysis and Human M1 Macrophage Polarization by Regulating
1118 Proximal Signaling and Akt2 Activation. Cell Rep *16*, 2442-2455.
1119 10.1016/j.celrep.2016.07.060.
1120 80. Heery, D.M., Kalkhoven, E., Hoare, S., and Parker, M.G. (1997). A signature motif
1121 in transcriptional co-activators mediates binding to nuclear receptors. Nature *387*,
1122 733-736. 10.1038/42750.
1123 81. Ludwig, C.H., Thurm, A.R., Morgens, D.W., Yang, K.J., Tycko, J., Bassik, M.C.,
1124 Glaunsinger, B.A., and Bintu, L. (2023). High-throughput discovery and
1125 characterization of viral transcriptional effectors in human cells. Cell Syst *14*, 482-
1126 500 e488. 10.1016/j.cels.2023.05.008.
1127 82. Davey, N.E., Van Roey, K., Weatheritt, R.J., Toedt, G., Uyar, B., Altenberg, B.,
1128 Budd, A., Diella, F., Dinkel, H., and Gibson, T.J. (2012). Attributes of short linear
1129 motifs. Mol Biosyst *8*, 268-281. 10.1039/c1mb05231d.
1130 83. Simonetti, L., Nilsson, J., McInerney, G., Ivarsson, Y., and Davey, N.E. (2023).
1131 SLiM-binding pockets: an attractive target for broad-spectrum antivirals. Trends
1132 Biochem Sci *48*, 420-427. 10.1016/j.tibs.2022.12.004.
1133 84. DeCaprio, J.A. (1999). The role of the J domain of SV40 large T in cellular
1134 transformation. Biologicals *27*, 23-28. 10.1006/biol.1998.0173.
1135 85. Sternsdorf, T., Jensen, K., Reich, B., and Will, H. (1999). The nuclear dot protein
1136 sp100, characterization of domains necessary for dimerization, subcellular
1137 localization, and modification by small ubiquitin-like modifiers. J Biol Chem *274*,
1138 12555-12566. 10.1074/jbc.274.18.12555.
1139 86. Everett, R.D., Boutell, C., McNair, C., Grant, L., and Orr, A. (2010). Comparison
1140 of the biological and biochemical activities of several members of the
1141 alphaherpesvirus ICP0 family of proteins. J Virol *84*, 3476-3487.
1142 10.1128/JVI.02544-09.
1143 87. Aird, E.J., Rabl, J., Knuesel, T., Scherpe, L., Boehringer, D., Corn, J.E. (2024).
1144 SP110 sequestration of SP100 protects against toxic filaments during innate
1145 immune signaling. bioRxiv preprint.
1146 88. Monaco, G., Lee, B., Xu, W., Mustafah, S., Hwang, Y.Y., Carre, C., Burdin, N.,
1147 Visan, L., Ceccarelli, M., Poidinger, M., et al. (2019). RNA-Seq Signatures
1148 Normalized by mRNA Abundance Allow Absolute Deconvolution of Human
1149 Immune Cell Types. Cell Rep *26*, 1627-1640 e1627.
1150 10.1016/j.celrep.2019.01.041.
1151 89. Isaac, A., Wilcox, K.W., and Taylor, J.L. (2006). SP100B, a repressor of gene
1152 expression preferentially binds to DNA with unmethylated CpGs. J Cell Biochem
1153 *98*, 1106-1122. 10.1002/jcb.20841.
1154 90. Zhang, X., Zhao, D., Xiong, X., He, Z., and Li, H. (2016). Multifaceted Histone H3
1155 Methylation and Phosphorylation Readout by the Plant Homeodomain Finger of
1156 Human Nuclear Antigen Sp100C. J Biol Chem *291*, 12786-12798.
1157 10.1074/jbc.M116.721159.
1158 91. Johnson, C.L., and Gale, M., Jr. (2006). CARD games between virus and host
1159 get a new player. Trends Immunol *27*, 1-4. 10.1016/j.it.2005.11.004.
1160 92. Mehta, S., Cronkite, D.A., Basavappa, M., Saunders, T.L., Adiliaghdam, F.,
1161 Amatullah, H., Morrison, S.A., Pagan, J.D., Anthony, R.M., Tonnerre, P., et al.

(2017). Maintenance of macrophage transcriptional programs and intestinal homeostasis by epigenetic reader SP140. Sci Immunol *2*. 10.1126/sciimmunol.aag3160.

93. Amatullah, H., Fraschilla, I., Digumarthi, S., Huang, J., Adiliaghdam, F., Bonilla, G., Wong, L.P., Rivard, M.E., Beauchamp, C., Mercier, V., et al. (2022). Epigenetic reader SP140 loss of function drives Crohn's disease due to uncontrolled macrophage topoisomerases. Cell *185*, 3232-3247 e3218. 10.1016/j.cell.2022.06.048.

94. Ba Abdullah, M.M., Palermo, R.D., Palser, A.L., Grayson, N.E., Kellam, P., Correia, S., Szymula, A., and White, R.E. (2017). Heterogeneity of the Epstein-Barr Virus (EBV) Major Internal Repeat Reveals Evolutionary Mechanisms of EBV and a Functional Defect in the Prototype EBV Strain B95-8. J Virol *91*. 10.1128/JVI.00920-17.

95. Satija, R., Farrell, J.A., Gennert, D., Schier, A.F., and Regev, A. (2015). Spatial reconstruction of single-cell gene expression data. Nat Biotechnol *33*, 495-502. 10.1038/nbt.3192.

96. Yu, G., Wang, L.G., Han, Y., and He, Q.Y. (2012). clusterProfiler: an R package for comparing biological themes among gene clusters. OMICS *16*, 284-287. 10.1089/omi.2011.0118.

97. Mootha, V.K., Lindgren, C.M., Eriksson, K.F., Subramanian, A., Sihag, S., Lehar, J., Puigserver, P., Carlsson, E., Ridderstrale, M., Laurila, E., et al. (2003). PGC-1alpha-responsive genes involved in oxidative phosphorylation are coordinately downregulated in human diabetes. Nat Genet *34*, 267-273. 10.1038/ng1180.

98. Schroedinger, L. The PyMOL Molecular Graphics System, Version 3.1.

99. White, R.E., Calderwood, M.A., and Whitehouse, A. (2003). Generation and precise modification of a herpesvirus saimiri bacterial artificial chromosome demonstrates that the terminal repeats are required for both virus production and episomal persistence. The Journal of general virology *84*, 3393-3403. 10.1099/vir.0.19387-0.

100. White, R.E., Wade-Martins, R., Hart, S.L., Frampton, J., Huey, B., Desai-Mehta, A., Cerosaletti, K.M., Concannon, P., and James, M.R. (2003). Functional delivery of large genomic DNA to human cells with a peptide-lipid vector. The Journal of Gene Medicine *5*, 883-892. 10.1002/jgm.420.

Supplemental Figures:

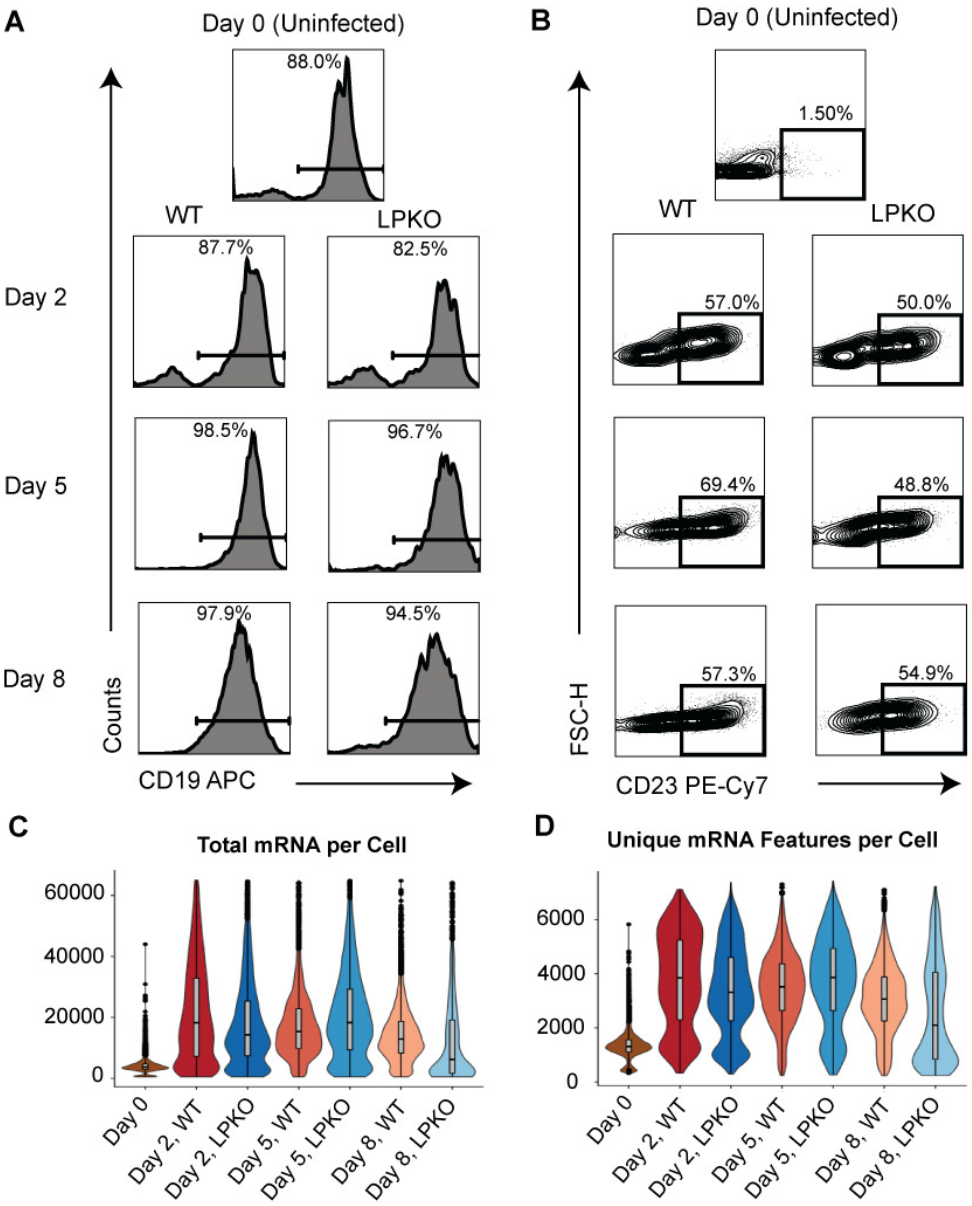

Supplemental Figure 1. Quality control of samples and scRNAseq libraries. A. Histogram of CD19 expression for each sample prior to collection. **B.** CD23 expression for each sample prior to collection. **C.** Total mRNA molecules read per cells in each sample. **D.** Total unique mRNA molecules per cell in each sample.

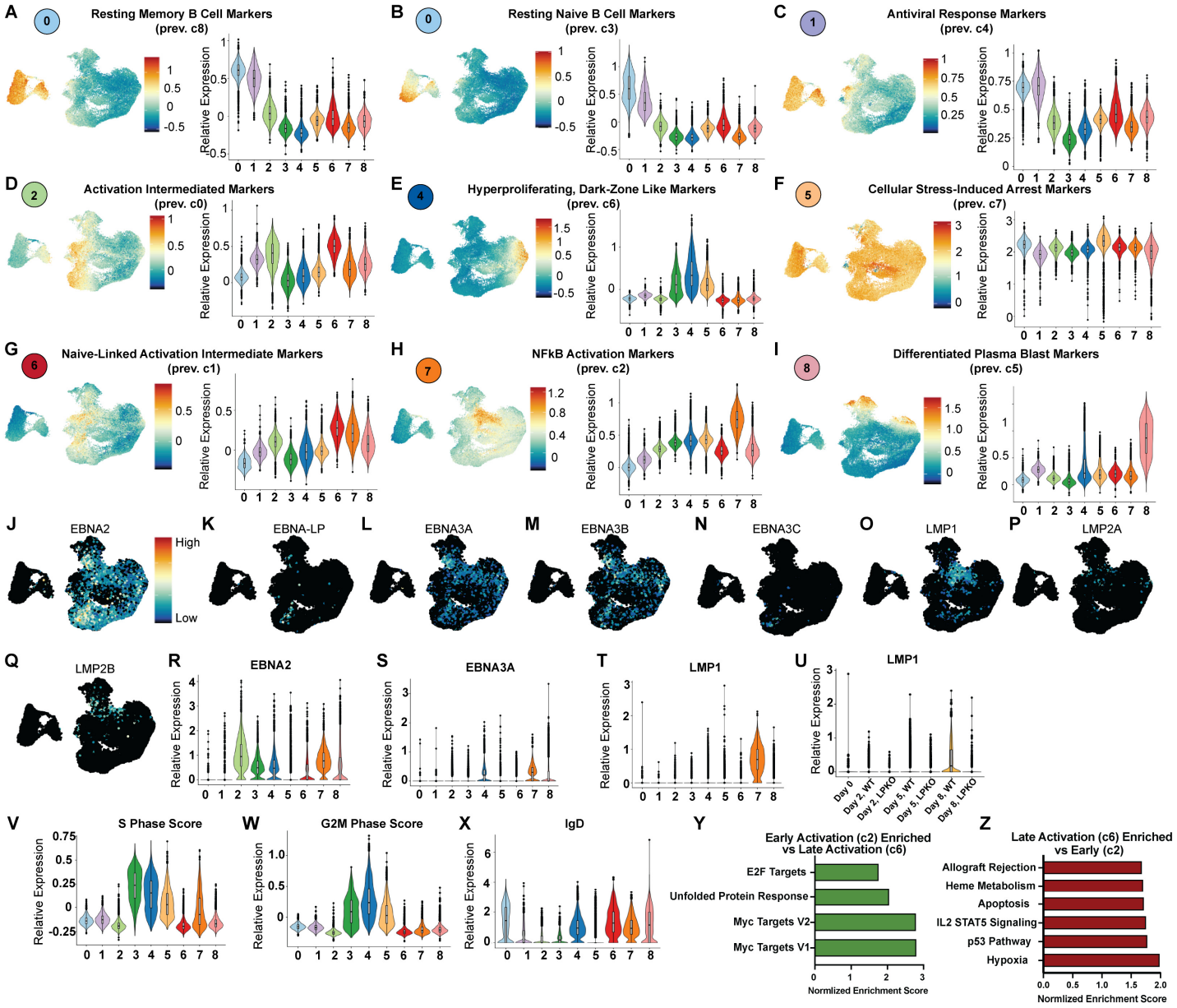

Supplemental Figure 2. Identified clusters correlate with EBV-induced cell states, viral gene expression, and cell cycle phase. Module scores based on top 100 differentially expressed genes for each previously identified B95-8 associated subpopulation**.** Umaps highlight cells with highest expression of indicated markers. Violin plot indicates relative expression of markers across clusters. The corresponding cluster number in prior publications (Sorelle, et al.) is indicated for reference. **A**. Resting Memory B cell Markers. **B.** Resting Naïve B cell Markers. **C.** Sensing/Antiviral Response Markers. **D.** Activation Intermediate Markers. **E.** Hyperproliferation/Dark Zone Like Markers. **F.** Cellular Stress-Induced Arrest Markers. **G.** Naïve-linked Activation intermediate Markers. **H**. NFκB-High/Light Zone Markers. **I.** Differentiated/Plasmablast State Markers. **J**. Umap of viral latency gene EBNA2 across all cells. **K.** EBNA-LP. **L.** EBNA3A. **M.** EBNA3B. **N.** EBNA3C. **O.** LMP1. **P.** LMP2A. **Q.** LMP2B. **R.** Violin plot of relative expression of viral gene EBNA2 across cluster. **S.** EBNA3A. **T.** LMP1. **U.** Violin plot of LMP1 expression by sample. **V.** Relative enrichment of S phase score across clusters. **W.** G2M phase score. **X.** Relative enrichment of IgD across clusters. **Y.** Significantly enriched (FDR q-value < 0.05) GSEA Hallmark pathways in Early Activation state compared to Late. **Z.** Enriched in Late compared to Early.

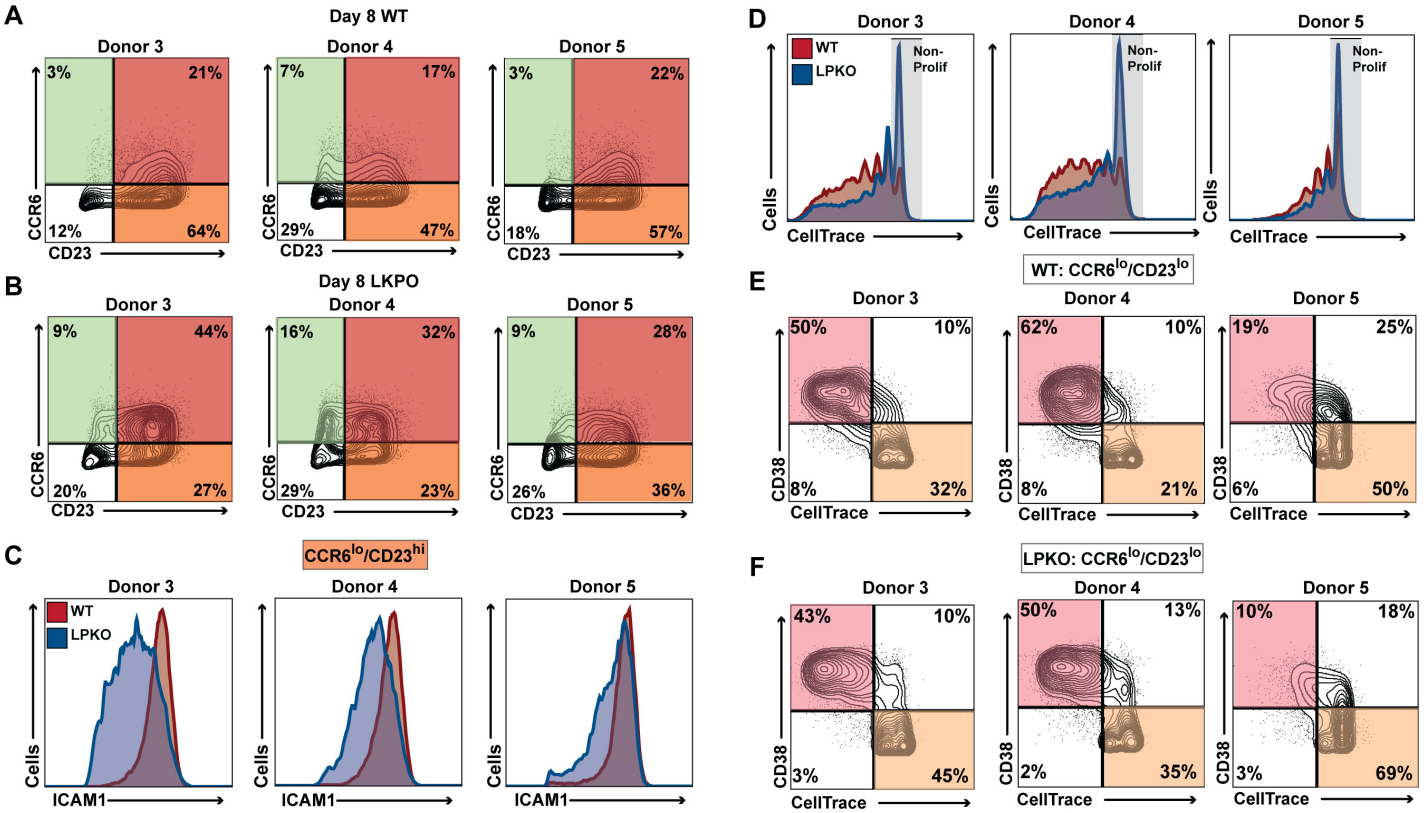

Supplemental Figure 3. Validation of scRNAseq data by flow cytometry in additional donors. Flow staining for CCR6 and CD23 8 days post-infection in additional donors infected with WT (**A**) or LPKO virus (**B**). Quadrant color corresponds to cell states that can be distinguished as depicted Figure 2E. **C**. Histograms comparing expression of ICAM1 protein (proxy for LMP1) between WT and LPKO infected cells in $CCR6^{lo}/CD23^{hi}$ population. **D.** Histogram of CellTrace stain, which is diluted during each cell division. Grey area indicates cells that have not undergone division. Separation of $CCR6^{lo}/CD23^{lo}$ populations in WT (**E**) and LPKO (**F**) infection by CD38 and CellTrace to distinguish Differentiated cells from Stressed cells. Histograms are scaled as percent of maximum count (modal).

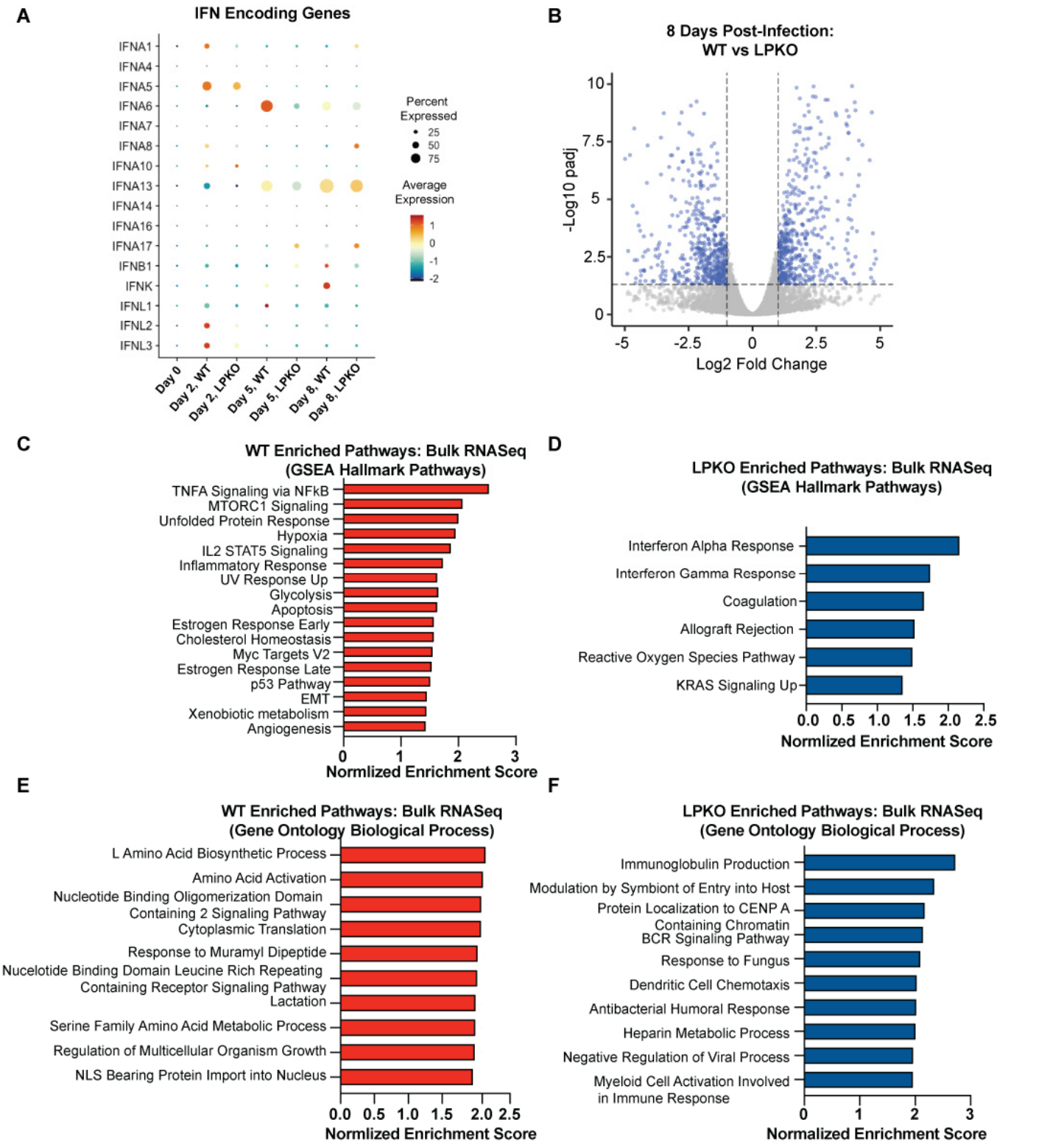

Supplemental Figure 4. Differential gene expression analysis in bulk RNAseq data 8 days post infection corroborates scRNA-seq data. A. Expression of genes encoding IFN detectable in scRNAseq time course samples. **B.** Volcano plot of differentially expressed genes between WT and LPKO samples. Gene sets enriched in WT infected cells compared to LPKO (**C**) and LPKO infected cells compared to WT (**D**) by GSEA analysis using Hallmark pathways by bulk RNA-seq. All gene sets with false discover rate (FDR q-value) less than 0.05 are plotted. Higher absolute value of Normalized Enrichment Score correlates with stronger enrichment. Gene sets enriched in WT infected cells compared to LPKO (**E**) and LPKO compared to WT (**F**) by GSEA analysis using Gene Ontology Biological Processes. The top 10 non-redundant enriched pathways with the highest Normalized Enrichment Score and FDR q-value less than 0.05 are shown.

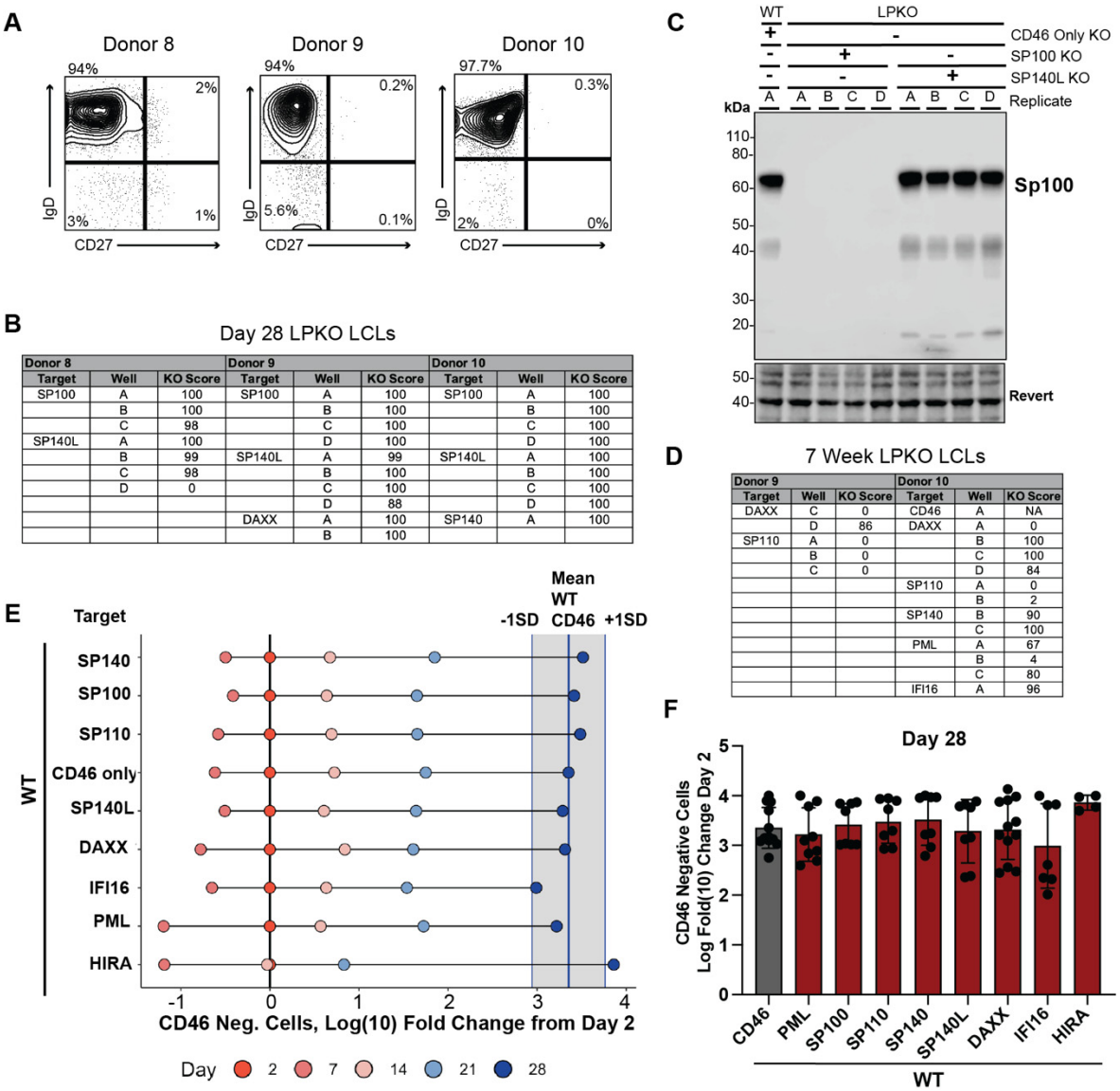

Donor 8			Donor 9			Donor 10		
Target	Well	KO Score	Target	Well	KO Score	Target	Well	KO Score
SP100	A	100	SP100	A	100	SP100	A	100
	B	100		B	100		B	100
	C	98		C	100		C	100
SP140L	A	100		D	100		D	100
	B	99	SP140L	A	99	SP140L	A	100
	C	98		B	100		B	100
	D	0		C	100		C	100
				D	88		D	100
			DAXX	A	100	SP140	A	100
				B	100			

Donor 9			Donor 10		
Target	Well	KO Score	Target	Well	KO Score
DAXX	C	0	CD46	A	NA
	D	86	DAXX	A	0
SP110	A	0		B	100
	B	0		C	100
	C	0		D	84
			SP110	A	0
				B	2
			SP140	B	90
				C	100
			PML	A	67
				B	4
				C	80
			IFI16	A	96

Supplemental Figure 5. Loss of *SP100* and *SP140L* does not impact outgrowth of WT EBV infected naïve B cells. A. Purity of isolated CD19 positive naïve B cell fractions for donors in screen. **B.** Knockout score for each LPKO LCL generated by 28 days post infection. **C.** Log(10) Fold Change from Day 2 of the total number of CD46 negative cells for each condition 2, 7-, 14-, 21-, and 28-days post-infection. Dark turquoise line represents the mean number of CD46 negative cells in CD46 only control WT infected cells 28 days post infection. **D.** Total number of CD46 negative cells 28 days post infection for each condition plotted as log fold change from 2 days post infection. P values calculated by one-way ANOVA with multiple comparisons. ** indicates p-values <0.01. **E.** Knockout score of LPKO LCLs generated after a total of seven weeks in culture, significantly delayed outgrowth compared to rescued LPKO LCLs and WT LCLs. **F.** Western blot for Sp100 protein expression in LPKO LCLs with *SP100* KO or *SP140L* KO from donor 3. Molecular weight in kDa is indicated.

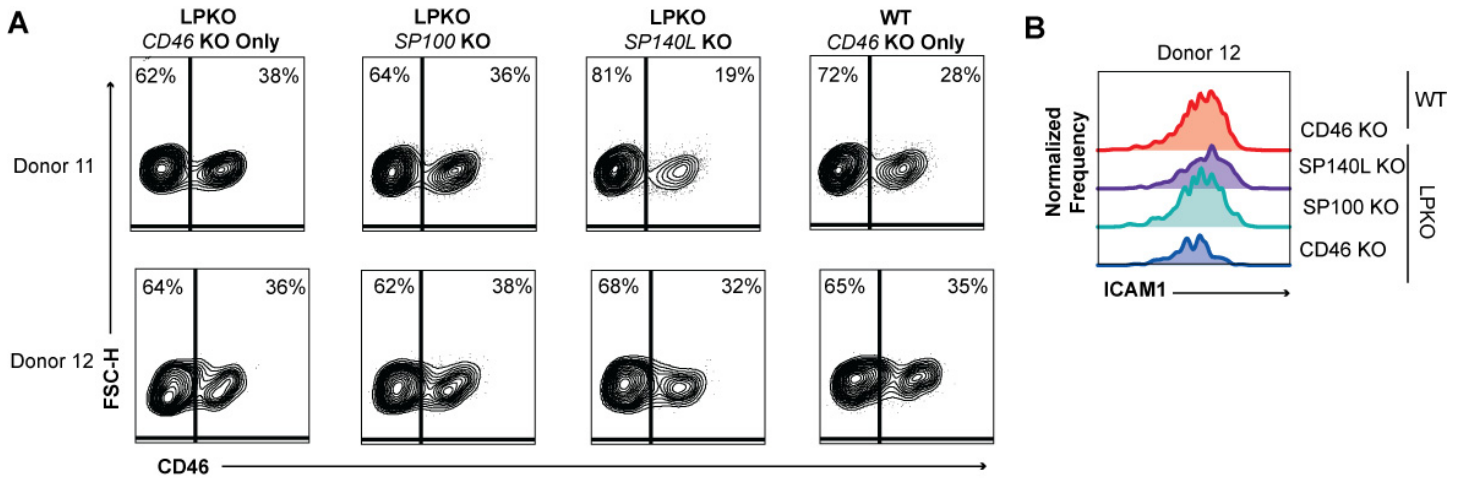

Supplemental Figure 6. RNAseq samples for *SP100* and *SP140L* knockout. A. CD46 negative and positive populations for each RNAseq sample at time of collection. **B.** ICAM1 expression in each sample from second donor not shown in Fig 6.

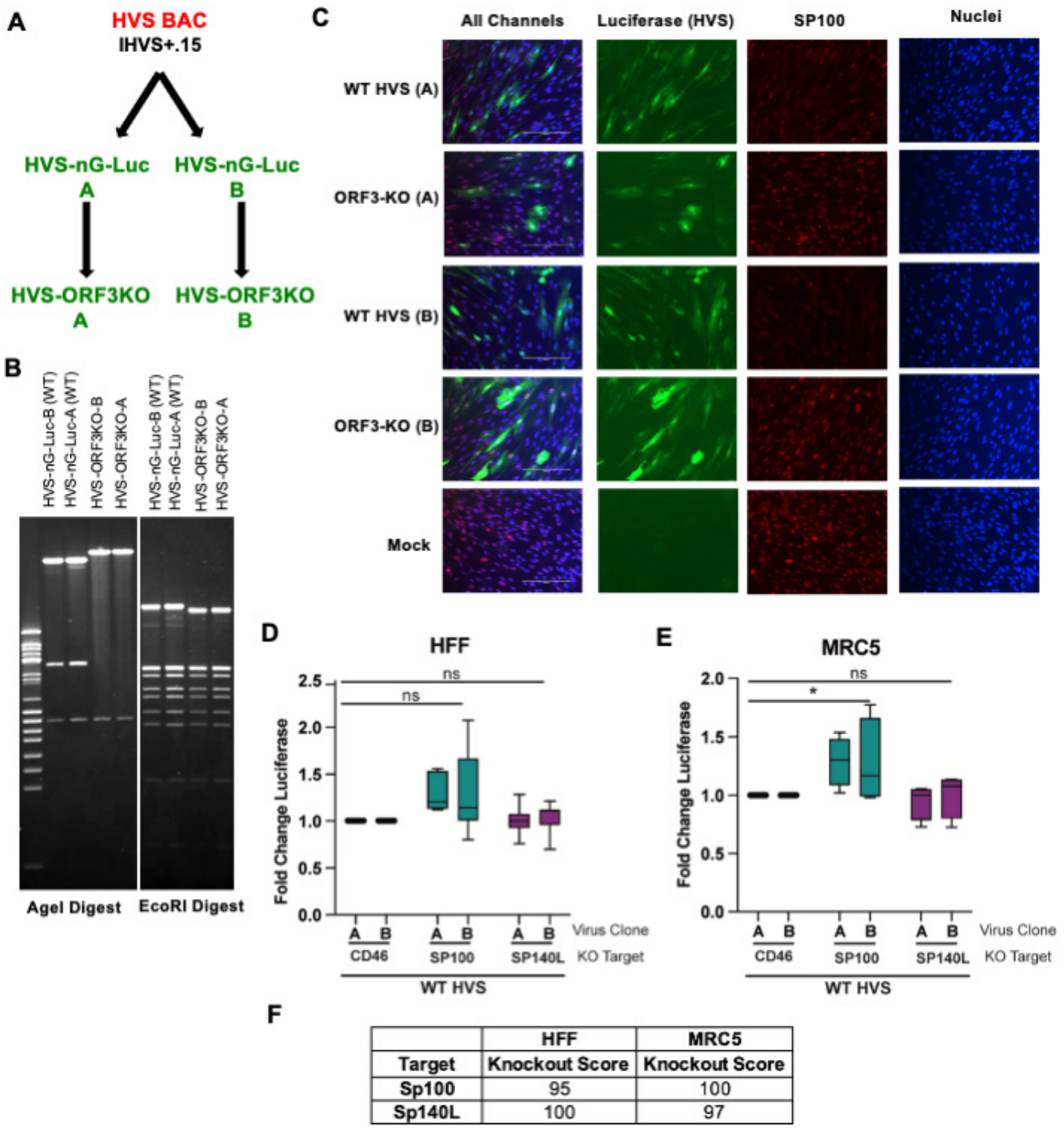

F

	HFF	MRC5
Target	Knockout Score	Knockout Score
Sp100	95	100
Sp140L	100	97

Supplemental Figure 7. *SP100* and *SP140L* loss has minimal effect on wild type HVS. A. Flow chart showing recombineering steps to generate the recombinant HVSs used in this study. Green indicates viruses with nGreenLuciferase (nGL-Luc) inserted. **B.** Restriction digest of WT HVS and ORF3-KO BACs confirming insertion of stop codon in ORF3-KO virus genome. **C**. Immunofluorescence of HFF cells infected with WT and ORF3-KO viruses. Green indicates nGreenLuciferase expression encoded in viral genome. Red indicates staining for Sp100. Blue indicates stained DNA. **D.** Relative luciferase expression in HFF knockout cells infected with WT HVS. **E.** MRC5 cells. P values calculated by two-way ANOVA with multiple comparisons. * Indicates p-values <0.05. **F.** Validation of SP100 and SP140L knockout by gDNA sequencing.